The Pennsylvania State University

The Graduate School

Department of Civil and Environmental Engineering

SHRINKAGE CHARACTERISTICS OF ALKALI-ACTIVATED SLAG CEMENTS

A Thesis in

Civil Engineering

by

Christopher Paul Cartwright

Submitted in Partial Fulfillment
of the Requirements
for the Degree of

Master of Science

May 2014

The thesis of Christopher Cartwright was reviewed and approved* by the following:

Aleksandra Radlińska
Assistant Professor of Civil and Environmental Engineering
Thesis Co-Adviser

Farshad Rajabipour
Assistant Professor of Civil and Environmental Engineering
Thesis Co-Adviser

Maria Lopez de Murphy
Associate Professor of Civil and Environmental Engineering

Peggy Johnson
Professor of Civil and Environmental Engineering
Head of the Department of Civil and Environmental Engineering

*Signatures are on file in the Graduate School

ABSTRACT

The annual production of Portland cement concrete exceeds 10^{10} tonnes/year. This large production volume has resulted in high energy consumption and emissions (e.g., CO_2) harmful to the environment. In addition, the aging infrastructure in developed countries coupled with shrinking financial resources for repair and renewal of infrastructure has resulted in much greater need to improve the durability and extend the service life of concrete structures. A growing incentive to develop durable, highly recycled, energy efficient and environmentally friendly concrete materials has initiated research on alkali-activated concretes.

Alkali-activated slag (AAS) utilizes blast furnace slag, an industrial byproduct of steel manufacturing, as a full (100%) replacement of Portland cement in concrete. AAS concrete has a low embodied energy, low CO_2 footprint, and equivalent or better strengths in comparison with ordinary Portland cement (OPC) concrete. AAS also has better durability against fire, chloride-induced corrosion, and chemical (e.g., acid, sulfate) attack. On the other hand, one of the most significant conundrums impeding the implementation of AAS is their volumetric instability. Specifically, AAS concretes are prone to significant shrinkage as a result of drying, carbonation, and self-desiccation and have shown a high risk of cracking.

The main objective of this research is focused on characterizing and understanding shrinkage deformations of AAS. It provides an unprecedented detailed study of the development of several AAS mortar mixtures and characterizes their susceptibility to the different types of shrinkage (drying, carbonation, and autogenous).

It was found that AAS mixtures, with comparable strength to OPC, show a higher autogenous and drying shrinkage. A lower elastic stiffness, higher degree of saturation, and potentially higher chemical shrinkage contribute to the high autogenous shrinkage of AAS. A lower elastic stiffness of mixtures activated solely by NaOH leads to a larger drying shrinkage. At

each relative humidity, AAS mixtures lose more mass and have larger drying shrinkage deformations than OPC mixtures, regardless of the drying rate. However, the ultimate drying shrinkage values of AAS are dependent on the drying rate as these materials shrink more when the relative humidity is decreased gradually instead of rapidly. The carbonation of AAS materials increases their drying shrinkage deformations. At high relative humidities (70% RH), creep plays a significant role in the drying shrinkage of AAS. The degree of saturation of AAS mixtures upon drying is lower than that of OPC and does not contribute to high drying shrinkage strains. Finally, after adjusting for the degree of hydration, the average chemical shrinkage of AAS paste is determined as 0.253 ml/g_{slag}. This is 3.95 times larger than the chemical shrinkage of Portland cement, and contributes directly to the large autogenous shrinkage of AAS materials.

TABLE OF CONTENTS

LIST OF FIGURES

LIST OF TABLES

ACKNOWLEDGEMENTS

I would like to offer full appreciation and gratitude to my two thesis advisers, Dr. Farshad Rajabipour and Dr. Aleksandra Radlińska. Their guidance, patience, and friendship during my undergraduate and graduate careers went far beyond the research and publications. I would like to also thank Dr. Maria Lopez de Murphy for participating as a member of my thesis committee. The financial support provided by NSF under Award CMMI #1265789 must also be recognized.

I'd like to especially acknowledge the help of two fellow graduate students, Mr. Jared Wright and Mr. Cory Kramer, who provided valuable scientific insight as well as emotional support during my career at Penn State. It would not have been remotely possible to complete this research without the help of Mr. Dan Fura. I am also appreciative of the help from research colleagues and friends in the lab: Mr. Greg Bruan, Mr. Hailong Ye, Mr. Yanbo Huang, and Mr. Hamed Maraghechi, among many others. I am also thankful to my great friends from my undergraduate studies at Penn State.

Finally, I would like to express my sincere gratitude to my family for their unconditional love and support. I am indebted to my brother, sisters, and girlfriend for their love and patience during my time as a graduate researcher. I am especially thankful to my parents who, from the beginning, instilled the qualities of love, discipline, and ambition in me.

Chapter 1

Objectives and Organization

1.1 Introduction

Concrete is a composite material in which aggregates (quarried) are bound together using a mixture of Portland cement and water. The mixture hardens and gains strength over time. Portland cement is produced by heating ground limestone and a source of silica (sand and/or clay) in a rotary kiln at temperatures up to 1550°C, resulting in an energy intensive process (embodied energy = 5.7MJ/kg) with a large CO_2 footprint (0.95kg CO_2/kg cement) (Mindess et al. 2003, Marinshaw and Wallace, 1994). The annual production of concrete exceeds 10^{10} tonnes/year, more than all other manmade materials combined (Ashby, 2009). This large production rate creates a large carbon footprint for Portland cement, resulting in approximately 5% of the world's total anthropogenic green house gas (GHG) emissions (Damtoft et al. 2008). The aging infrastructure in developed countries, coupled with shrinking financial resources for repair and renewal of the current infrastructure, has resulted in a much greater need to improve the durability and extend the service life of concrete structures. This underlines the need for evaluating more environmentally friendly products to replace Portland cement in concrete. A growing incentive to develop durable, highly recycled, energy efficient and environmentally friendly concrete materials has initiated research on alkali-activated concretes.

Multiple products have been researched up to date to partially or fully replace Portland cement in concrete. Research has shown (Ben Haha et al. 2011, Shi et al. 2006, Radlinska et al. 2012) that industrial waste products, e.g. blast furnace slag from steel manufacturing or fly ash from coal combustion, can be used to successfully produce a Portland cement-free concrete.

Alkali-activated slag (AAS) is a promising product, proven to have cementitious properties capable of possessing compressive strengths equal to or higher than those of OPC.

Certain durability aspects of AAS have been shown to be quite favorable compared to OPC. Shi et al. (2006) has shown that AAS materials have lower chloride and water permeability and a higher resistance to attack by acids, sulfates, and fires. However, one durability aspect limiting the usage of AAS is its volumetric instability. For example, many authors (Shi et al. 2006, Melo Neto et al. 2008, Douglas et al. 1992, Bakharev et al. 2000, Palacios and Puertas 2007, Cincotto et al. 2003) have shown that AAS concrete can have up to 2.5 times larger shrinkage deformations than PC mixtures. This high shrinkage poses concerns since it can result in cracking when concrete members are restrained from shrinking freely (e.g., in pavements and bridge decks). Formation of cracks allows salts and other aggressive chemicals to penetrate the concrete, corrode the reinforcing steel, and significantly reduce the service life of the structure.

The shrinkage mechanisms of AAS systems remain relatively unknown as certain types of shrinkage (e.g., chemical and carbonation) have yet to be properly measured and analyzed. Many of the current shrinkage test methods are either not standardized or not directly applicable to AAS materials, thus other methods need to be explored. Furthermore, a comprehensive study that investigates every mechanism (i.e., creep, modulus of elasticity, pore size distribution, and bulk modulus) that can potentially cause shrinkage in AAS systems has not been performed. Several attempts to mitigate shrinkage in AAS have failed due to a lack of understanding of these shrinkage mechanisms. This research aims to properly measure, investigate, and mitigate the AAS shrinkage problem. Doing so can provide tremendous benefits towards producing durable AAS concretes and a viable replacement for OPC concrete.

1.2 Research Objectives

The main objective of this research is focused on measuring, understanding, and mitigating the large shrinkage deformations of AAS. The first step is to correctly measure each shrinkage type individually to determine how much AAS materials shrink. Subsequently, determining which parameters govern each type of shrinkage will provide insight on why these materials have such large deformations. Bridging such knowledge gaps will then result in developing efficient shrinkage mitigation tools for alkali-activated concretes and create a viable alternative for OPC concrete.

1.3 Research Approach

This research was conducted based on four AAS mixtures and the characterization of their mechanical and shrinkage properties. The study provides comparisons with properties of an OPC mixture of similar initial porosity. Depending on the test performed, paste or mortar was used. Four AAS mixtures and a control OPC mixture were designed using a constant volumetric liquid (water + activator) to solid (slag or cement) ratio of 1.30, yielding an initial binder porosity of 56.5%. Binder porosity was calculated assuming 100% hydration of cementitious material, 1:1 volume consumption of the liquid to solid, and evaporation of excess liquid after the entirety of the cement (or slag) powder had reacted. For the control OPC mixture, this is equivalent to a mass-based w/c = 0.414. For the AAS mixtures, the mass-based liquid to solid ratio was in the range 0.489-0.510, depending on the concentration and density of the alkali activating solutions (Table 1-1). A constant volumetric liquid to binder ratio creates equivalent initial binder porosities across all five mixtures that allows for easy comparisons of paste and mortar properties.

Table 1-1. Naming system for mixtures

Mix ID (*Description*)	$n = (SiO_2/Na_2O)$ molar-based	pH	Density (g/cc)
AAS1 (*Lower SiO_2 Na-Si*)	0.41	14.31	1.09
AAS2 (*Higher SiO_2 Na-Si*)	1.22	13.78	1.13
AAS3 (*2M NaOH*)	0	14.30	1.04
AAS4 (*4M NaOH*)	0	14.60	1.09

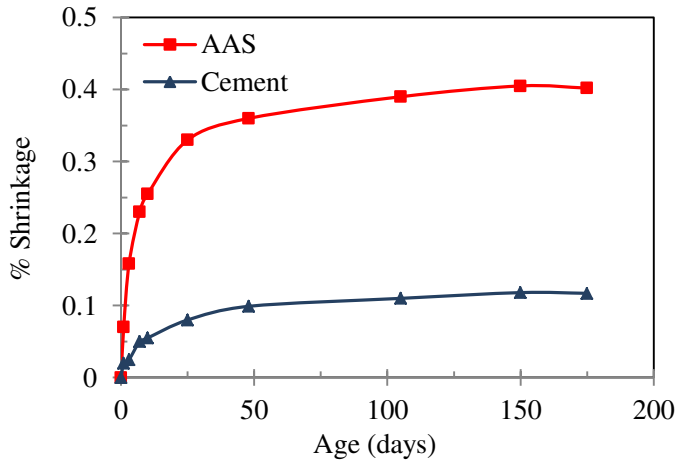

Figure 1-1: Typical Age vs. Shrinkage graph. Source: Palacios and Puertas (2007)

Table 1-1 provides a simple naming system for the mixtures throughout the entire project. The majority of the research will focus on comparing shrinkage strains and other parameters of the four AAS mixtures to OPC. Figure 1-1 provides the typical format of an age vs. shrinkage graph that will be presented throughout this report. These types of graphs will provide easy comparisons of several types of shrinkage tests of the four AAS mixtures and OPC. The following tests are performed on all mixtures:

- ASTM C1437: Standard Test Method for Flow of Hydraulic Cement Mortar

- ASTM C109: Standard Test Method for Compressive Strength of Hydraulic Cement Mortars
- ASTM C403: Standard Test Method for Time of Setting of Concrete Mixtures by Penetration Resistance
- ASTM C596: Standard Test Method for Drying Shrinkage of Mortar Containing Hydraulic Cement
- ASTM C1698: Standard Test Method for Autogenous Strain of Cement Paste and Mortar
- Degree of Hydration of Blast Furnace Slags: Procedure adopted from Luke and Glasser (1987)
- Chemical Shrinkage of Hydraulic Cements: Procedure adopted from Sant et al. (2005)

The first three tests listed (mortar flow, time of setting, and compressive strength) characterize the development of AAS and OPC mixtures. Shrinkage deformations were quantified by running drying shrinkage (ASTM C596), autogenous shrinkage (ASTM C1698), and chemical shrinkage (via the buoyancy method (Sant et al. 2005)) on each mixture. The degree of hydration of every AAS mixture was measured (via selective acid dissolution (Luke and Glasser, 1987) to normalize the results of the chemical shrinkage.

Drying shrinkage of non-standardized "mini-bars" in environmental chambers will be measured under various relative humidities as well as compressed dry nitrogen (N_2) and air purge. These results will provide insight on the role carbonation plays in the drying shrinkage of AAS materials.

1.4 Outline

This thesis is presented in five (5) remaining chapters. **Chapter 2** will provide the motivation and background on the characterizing the development and shrinkage of AAS systems. **Chapter 3** is a technical paper named "Shrinkage characteristics of alkali-activated slag cements" recently accepted by the ASCE Journal of Materials in Civil Engineering. This paper was initially a conference paper accepted and presented at the Third International Conference on Sustainable Construction Materials and Technologies on August 18-21, 2013. The paper was selected for recognition as an "Award Winning Paper" and sent to ASCE Journal of Materials in Civil Engineering for journal publication. **Chapter 4** is another technical paper named "Drying shrinkage of alkali-activated slag cements. Part 1: Characterization of drying shrinkage under various relative humidities" recently submitted to the Cement and Concrete Research journal. **Chapter 5** is a conference paper named "Measuring the chemical shrinkage of alkali-activated slag cements using the buoyancy method". This paper was accepted and presented at the Ninth International Conference on Creep, Shrinkage, and Durability Mechanics (CONCREEP-9) on September 22-25, 2013 in Cambridge, MA. Finally, **Chapter 6** will conclude the thesis proposal with research conclusions and future work. References are provided at the end of each respective chapter.

1.5 References

American Society for Testing and Materials (ASTM), "Standard Practice for Mechanical Mixing of Hydraulic Cement Pastes and Mortars of Plastic Consistency," ASTM International, ASTM C 305-12.

American Society for Testing and Materials (ASTM), "Standard Specification for Concrete Aggregates," ASTM International, ASTM C 33M-11a

American Society for Testing and Materials (ASTM), "Standard Specification for Slag Cement for Use in Concrete and Mortars." ASTM International, ASTM C989-10.

American Society for Testing and Materials (ASTM), "Standard Test Method for Compressive Strength of Hydraulic Cement Mortars," ASTM International, ASTM C 109M-11.

American Society for Testing and Materials (ASTM), "Standard Specification for Lightweight Aggregate for Internal Curing of Concrete," ASTM International, ASTM C 1761M-12.

American Society for Testing and Materials (ASTM), "Standard Test Method for Time of Setting of Concrete Mixtures by Penetration Resistance," ASTM International, ASTM C403M-08.

American Society for Testing and Materials (ASTM), "Standard Test Method for Drying Shrinkage of Mortar Containing Hydraulic Cement," ASTM International, ASTM C596.

American Society for Testing and Materials (ASTM), "Standard Test Method for Flow of Hydraulic Cement Mortar," ASTM International, ASTM C1437-07.

American Society for Testing and Materials (ASTM), "Standard Test Method for Autogenous Strain of Cement Paste and Mortar," ASTM International, ASTM 1698.

Ashby, M. (2009), Materials and the Environment, Elsevier, Inc, Burlington, MA

Bakharev, T., Sanjayan, J.G., Cheng, Y.B. (2000), "Effect of admixtures on properties of alkali-activated slag concrete." Cement and Concrete Research, 30, 1367-1374.

Ben Haha, M., Le Saout, G., Winnefeld, F., Lothenbach, B. (2011), Influence of activator type on hydration kinetics, hydrate assemblage and microstructural development of alkali activated blast furnace-slags. Cement and Concrete Research, 41 301-310.

Cincotto, M.A, Melo A. A., Repette, W.L. (2003), "Effect of different activators type and dosages and relation to autogenous shrinkage of activated blast furnace slag cement." In: G.

Grieve, G. Owens, Eds, Proc. 11th International Congress on the Chemistry of Cement, Durban, South Africa, (2003) 1878-1888.

Damtoft, J.S., Lukasik, J., Herfort, D., Sorrentino, D., Gartner, E.M. (2008), Sustainable development and climate change initiatives, Cement and Concrete Research, 38, 115-12.

Douglas, E., Bilodeau, A., Malhotra, V.M. (1992), Properties and durability of alkali-activated slag concrete, ACI Materials Journal, 89, 509-516.

Luke, K., Glasser, F.P. (1987), Selective dissolution of hydrated blast furnace slag cements, Cement and Concrete Research, Vol. 17, pp. 273-282.

Marinshaw, R., Wallace, D., (1994). "Emission factor documentation: Portland cement manufacturing." United States Environmental Protection Agency (EPA), www.epa.gov/ttn/chief/ap42/ch11/bgdocs/b11s06.pdf (accessed May 15, 2013).

Melo Neto, A.A, Cincotto, M.A., Repette, W. (2008) "Drying and autogenous shrinkage of pastes and mortars with activated slag cement." Cement and Concrete Research 38(4) 565-574.

Mindess, S., Young, J.F., Darwin, D. (2003), Concrete 2nd Ed., Prentice Hall, Upper Saddle River, New Jersey.

Palacios, M., Puertas, F. (2007), Effect of shrinkage-reducing admixtures on the properties of alkali-activated slag mortars and pastes, Cement and Concrete Research 37, 691–702.

Shi, C., Krivenko, P., Roy, D. (2006), Alkali-Activated Cements and Concrete, Taylor & Francis.

Sant, G., Lura, P., Weiss, J. (2005), Measurement of Volume Change in Cementitious Materials at Early Ages, Transportation Research Board.

Radlinska, A., Salera, M., Ernst, S., Yost, J., Rajabipour, F. (2012), "Linking material and structural response of alkali-activated fly ash binders." International Congress on Durability of Concrete.

Chapter 2

Background

2.1 Motivation

The popular controversy regarding climate change, our planet's sustainability, and the validity of each side's argument continues to reverberate around the world; however, scientific facts and reasoning have strongly suggested that climate change is indeed occurring at a rapid rate. Mehta (2002) claims that according to scientists, man-made climate change appears to be the greatest environmental challenge we face today. Figure 2-1 shows a yearly timeline of the earth's atmospheric CO_2 concentration from the Intergovernmental Panel on Climate Change (IPCC) (2001). Clearly, the planet's once constant CO_2 concentration has increased exponentially since the early 1900s. Just recently, Mother Nature has been providing warning signs to these occurrences. For example, since the 1990s, the Worldwatch Institute has noticed an unusually high number of extreme weather-related disasters in many parts of the world (Flavin and Tunali 1996). These facts strongly support the central idea that our planet is experiencing a "man-induced" global warming. In order to create a more sustainable planet and avoid further damage to the environment, humans need to reduce greenhouse gas emissions into the environment.

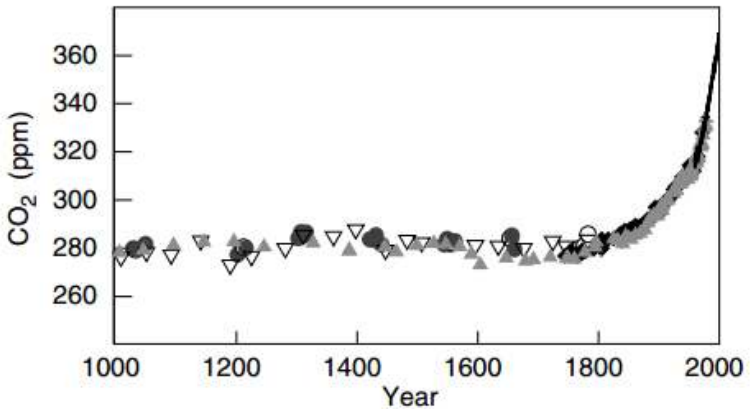

Figure 2-1: Yearly timeline of Earth's atmospheric CO2 concentration. Source: IPCC (2001)

Concrete production utilizes the most abundant natural materials present on the Earth's surface; however, the high temperatures (~1500°C) required during production of Portland cement in the kiln result in a significant energy use (embodied energy = 5.7MJ/kg of cement) and a large CO_2 footprint (0.95kg CO_2/kg of cement) (Mindess et al. 2003, Marinshaw and Wallace 1994). Altogether, cement production is responsible for approximately 5% of the total anthropogenic GHG emissions – roughly equivalent to the CO_2 output of the entire nation of Japan (Damtoft et al. 2008). This raises sustainability concerns and fosters significant interest in Portland cement-free binders, which will reduce the carbon footprint of concrete.

Every four years, the American Society of Civil Engineers (ASCE) prepares an updated condition assessment of the current state of America's infrastructure. Using a common school grading system, ASCE graded America's infrastructure in 2013 as a D+ (ASCE, 2013), adding that $3.6 trillion needs to be invested by 2020 to revive the infrastructure back to acceptable standards of quality. The durability of concrete plays a big role in the deteriorating infrastructure and must be improved to extend the service life of newly constructed infrastructure. Combined with the increasing need to recycle products and preserve our planets natural materials, more durable and eco-friendly binders need to be developed.

2.2 Ground Granulated Blast Furnace Slag

Multiple environmentally friendly products have been researched up to date to partially or fully replace Portland cement in concrete. Mehta (2002) defines the term industrial ecology as "recycling waste products of one industry by substituting them for the virgin raw materials of another industry, thereby reducing the environmental impact of both". Research has shown (Ben Haha et al. 2011, Shi et al. 2006, Radlinska et al. 2012) that industrial waste products, e.g. blast

furnace slag from steel manufacturing and fly ash from coal production, can be used to successfully produce a Portland cement-free concrete when activated by alkaline solution.

During steel production, iron ore, coke/coal, and limestone are mixed in a hot blast furnace where two materials, molten pig iron and molten slag, are produced (Siddique and Khan 2011). The denser pig iron (which is further processed to make steel) sinks to the bottom while the lighter molten slag floats on top and is periodically removed from the blast furnace (Figure 2-2). Once removed from the furnace, liquid slag is immediately quenched to a solid state by air granulation. The rapid quenching impedes the formation of crystals, and the resulting granular material comprises of about 95% amorphous calcium-alumino-silicate glass (Siddique and Khan 2011). Ground granulated blast furnace slag (GGBFS) is then produced by grinding this material into a fine powder (e.g., <45μm).

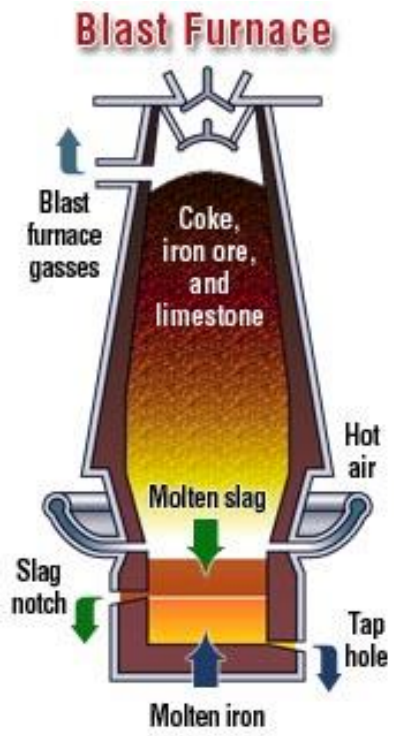

Figure 2-2: Display of a blast furnace and the removal of molten slag. Source: National Slag Association (2009)

GGBFS is a technically a glass (95% amorphous). A glass is defined as an amorphous material completely devoid of a long range ordered atomic structure (Shelby 2005). During production, a glass experiences what is known as "glass transition behavior", the tendency of the material to bypass crystallization during rapid cooling as its atomic structure remains disordered (amorphous) and mimics that of a "frozen liquid" (Shelby 2005). Rapid cooling from liquid to solid demotes nucleation and crystal formation which would occur under slower cooling rates (Shelby 2005).

The chemicals found in slag are quite similar to those seen in Portland cement; however, the quantities are dissimilar. The chemical composition of slag varies depending on the raw materials and furnace operation (Shi et al. 2006). Figure 2-3 shows the ternary diagram of SiO_2, Al_2O_3, and CaO (a typical diagram used in cement chemistry) of blast furnace slag and Portland cement. As shown, the CaO/SiO_2 ratio is different for the two materials. Pal et al. (2003) has suggested that a larger percentage of SiO_2 in slag reduces its reactivity in AAS materials. A larger concentration of SiO_2 would create more Si-O network forming bonds (discussed in the following section) in a glass (Shelby 2005) which would strengthen the glass and increase its resistance to corrosion and congruent dissolution, an unfavorable occurrence in the alkali activation process. Parameters that increase the reactivity of a slag include a high surface area, glass content, and increased CaO/SiO_2 (Shi et al. 2006). The chemical composition and particle size distribution of the slag used in this research are provided in Chapter 3.

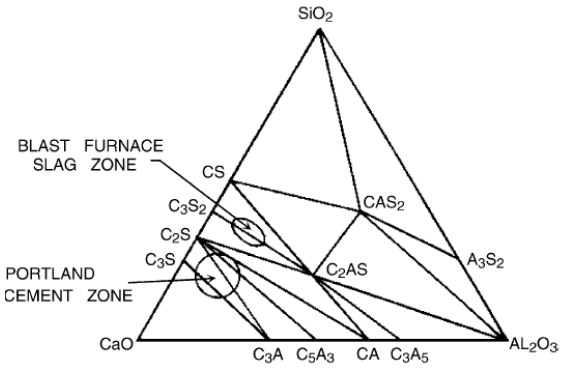

Figure 2-3: Ternary diagram of Portland cement and slag. Source: Pal et al. 2003

2.3 Alkali Activated Slag

Figure 2-4 shows the typical atomic structure of crystalline quartz and amorphous silica and soda-lime glass. In an amorphous glass, the silica atoms act as network-formers and provide the connectivity and strength of the glass. It is known that glassy siliceous materials are relatively stable at low and neutral pH and experience congruent dissolution at high pH (Shelby 2005). Congruent dissolution is the attack on network bonds in a glass from OH^- ions in the solution, resulting in dissolution of the glass. Figure 2-5 shows the dissolution rate of a silica glass vs. pH of the solution. This graph shows that the dissolution of glass is highly dependent on the pH of the solution. Alkali activation is the process of exposing an amorphous material (e.g., slag or fly ash) to a high pH environment to promote and accelerate the congruent dissolution of the material's Al-O, Si-O, and Ca-O bonds. The dissolved alumino-silicates can then react with water and the available calcium ions to form calcium silicate hydrate (C-S-H) and calcium-aluminum-silicate hydrate (C-A-S-H) gels that provide the binder phase in concrete (Ben Haha et al. 2011). When used as a partial replacement for Portland cement, the slag is dissolved by the pore solution (pH>12.5) of concrete that already has a high pH due to the presence of solid $Ca(OH)_2$, a byproduct of cement hydration. In Portland cement-free binders, the slag must be manually

activated by raising the pH of the mix water using alkali chemicals. Typical "activators" used to independently raise the pH include $Na_2O(SiO_2)_n$ (also known as "water glass"), NaOH, and Na_2CO_3. Wang (2000) has shown via XRD and NMR that sodium ions are simply present to balance the hydroxyl ions during the dissolution process and do not play an integral role in the formation or structure of C-S-H or C-A-S-H gel. The process of alkali activation of these amorphous materials allows for the successful development of a Portland cement-free binder.

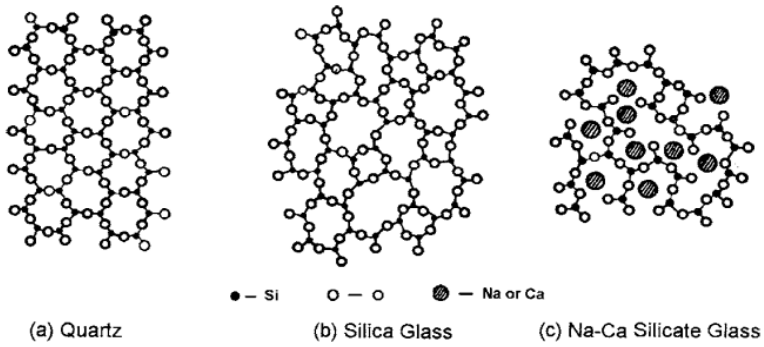

Figure 2-4: Atomic structure of quartz, silica glass, and soda-lime glass. Source: Shi et al. 2006

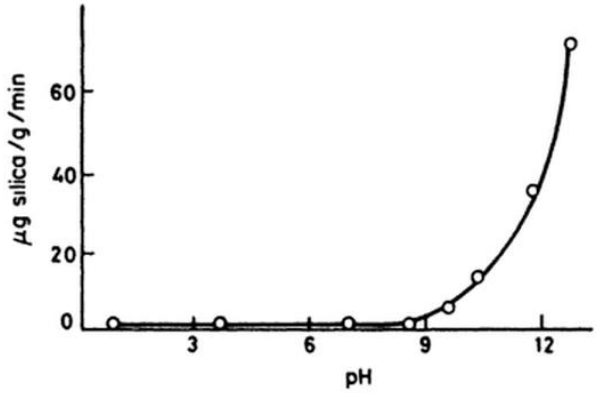

Figure 2-5: Dissolution rate of silica glass vs. pH of solution. Source: Paul (1990)

2.4 Microstructure Characteristics

Microstructure development of alkali-activated slag is quite different than that of ordinary Portland cement. As mentioned earlier, the amorphous slag dissolves in the high pH pore solution to release Ca^{2+} ions as well as aqueous aluminum (e.g., $Al(OH)_4^-$) and aqueous silica (e.g., $Si(OH)_4$). The activator type and dosage play a critical role in the strength development, pore structure, and degree of hydration of AAS pastes. NaOH and $Na_2O(SiO_2)_n$ were two activators tested in this research, thus previous work on these two activators will be reported and compared here.

It was reported (Ben Haha et al. 2011), that waterglass activated binders have a denser C-S-H structure and lower gel porosity than NaOH. This is most likely due to the slower slag hydration, which permits uniform precipitation of the gel into the open pore space. Conversely, NaOH activated binders produce rapid formation of hydration products that quickly clog the pore space and slow down further precipitation of C-S-H (Ben Haha et al. 2011). This creates a weaker, highly porous, and poorly distributed C-S-H gel (right side of Figure 2-6). The denser microstructure of waterglass activated binders (left side of Figure 2-6) would contain higher compressive strength than those activated by NaOH; however, the finer pore structure for waterglass activated binders may hold negative implications on its shrinkage performance as discussed later.

The degree of hydration of AAS systems have been reported (Ben Haha et al. 2011) to be significantly lower than traditional OPC pastes. NaOH activated binders initially hydrate quicker than waterglass activated binders and therefore have a higher degree of hydration (Figure 2-7) (Ben Haha et al. 2011). However, the slow, continuous hydration of water glass activated binders eventually matches the ultimate degree of hydration of NaOH activated binders (Ben Haha et al. 2011).

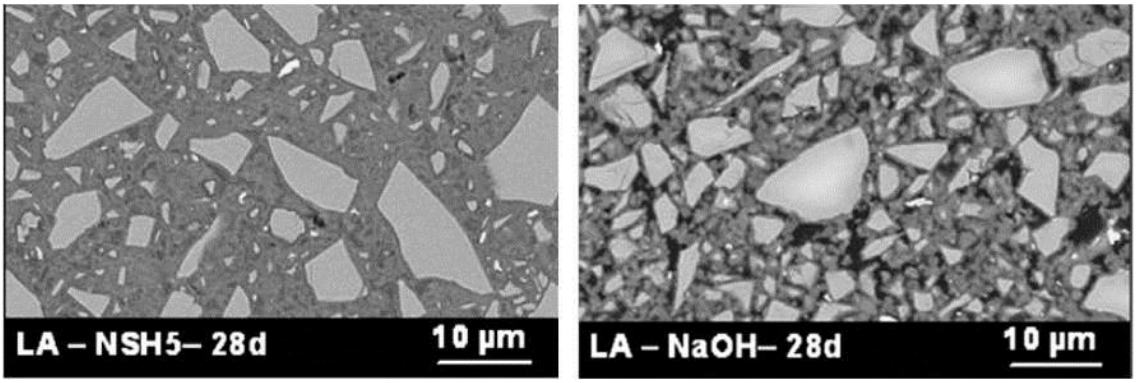

Figure 2-6: Microstructure after 28 days of waterglass (left) and NaOH (right) activated slag. Source: Ben Haha et al. 2011

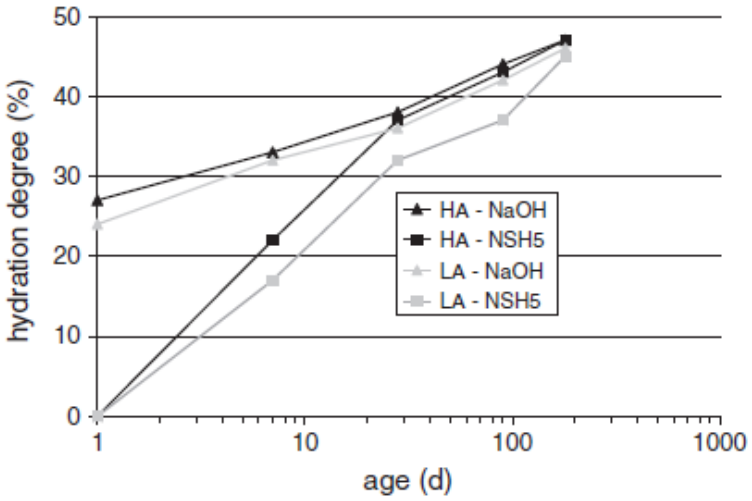

Figure 2-7: Hydration degree vs. Age of AAS pastes. Source: Ben Haha et al. 2011

2.5 Compressive Strength

It has been proven that AAS systems can be designed for compressive strengths comparable to, or even exceeding, the ordinary Portland cement (OPC) (Shi et al 2006, Fernandez-Jimenez et al. 1999, Palacios and Puertas 2007, Bakharev et al. 2000, Wang et al.

1994, Brough and Atkinson 2002, Krizan and Zivanovic 2002). Strength development of AAS pastes is highly dependent on the activator dosage and activator type used. It was generally found (Shi et al. 2006, Ravukimar et al. 2010) that an increased activator dosage resulted in higher pH and faster hydration. The type of activator, however, generally dictated the strength as $Na_2O(SiO_2)_n$ activated binders were found (Shi et al 2006, Fernandez-Jimenez 1999, Wang et al 1995, Wang et al. 1994) to have higher compressive strengths than NaOH activated binders.

2.6 Fresh Properties

Collins and Sanjayan (1999) measured the slump of AAS concrete activated by aqueous sodium silicate. They observed a lower workability in AAS than OPC and a significant slump loss after only 60 minutes. Shi et al. (2006) has also reported workability issues in AAS and that some conventional water reducing admixtures (WRA) used in OPC concrete are not as beneficial in AAS mixtures. However, conflicting reports from other scientists (Jolicoeur et al. 1992) have reported that certain WRAs do provide satisfactory results in improving the workability and flow of AAS mixtures.

2.7 Time of Setting

Time of setting is an important property of concrete materials as it tells how fast a paste is hydrating and, more elementary, how long (i.e. hours) a mixture remains in the plastic state. Time of setting for AAS systems has been measured with various results and consistencies. Chang (2003) reported that an increase in activator dosage and pH reduces both initial and final time of setting of AAS systems. Brough and Atkinson (2000) measured inconsistencies of setting

times with initial time of sets in the range from 2.75 to 4.25 hours and final time of sets in the range of 3.25 to 5.5 hours.

2.8 Elastic Modulus and Creep

Collins et al. (1999) measured and compared the elastic modulus and creep of AAS concrete to OPC concrete. They observed a 12% lower elastic modulus for AAS concretes (36.7 GPa) when compared to OPC concretes (41.7 GPa). They also noticed a higher creep (about 14%) in AAS systems. Shi et al. (2006) has also reported higher creep in AAS compared to OPC.

2.9 Durability

As discussed earlier in this chapter, the durability of concrete is essential to building structures with longer service lives in America's infrastructure. Therefore, before declaring AAS a marketable product, its durability must be evaluated. Certain AAS durability aspects have been reported favorably when compared to OPC. For example, Davidovits (1994) and Wu et al. (1993) both reported a lower water permeability for AAS concretes. Similarly, chloride permeability (and therefore chloride induced corrosion) through AAS has been shown to be lower than that of OPC (Shi et al. 2006). Shi et al. (2006) has suggested that this is most likely due to the refined pore structure of AAS pastes, which would create a lower coefficient of permeability. The resistance of AAS to other chemical attacks (i.e., sulfates and acids) has also been shown (Shi, 2003) to be superior when compared to OPC. The fire resistance of AAS concrete has also been observed (Shi et al., 2006) to be quite favorable when compared to OPC. Shi et al. (2006) have argued that this is possibly due to the lack of production of $Ca(OH)_2$ in AAS systems, which

decomposes in Portland cement at high temperatures and results in significant strength reductions.

Other durability aspects of AAS cements, however, have been shown to be inferior to OPC. The carbonation of AAS concrete has been shown (Bakharev et al., 2001) to be much more intense than what is seen in OPC. Bakharev et al. (2001) have reported significant compressive strength reductions in carbonated AAS concrete, while carbonated OPC concrete actually saw a slight increase in compressive strength. The drying shrinkage of AAS has also been studied and shown (Bakharev et al, 2000) to be much larger than the drying shrinkage observed in OPC. The remained of this literature background will present the findings on the shrinkage of AAS.

2.10 Shrinkage

The marketability and acceptance of alkali-activated concretes (AAC) in the industry have been hindered by concerns related to their durability against shrinkage cracking. High shrinkage strains become a durability problem since they can result in cracking when concrete members are restrained from shrinking freely (e.g., in pavements and bridge decks). These cracks allow salts and other aggressive chemicals to penetrate the concrete, corrode the reinforcing steel, and significantly reduce the service life of the structure.

2.10.1 Drying Shrinkage

As concrete is moist cured, it is assumed to be in a sealed environment and, therefore, at a relative humidity of 100%. However, the inevitable termination of moist curing places the concrete in direct contact with the ambient environment which is almost always at a relative humidity less than 100%. As the concrete adjusts to this change in humidity, the water in the

pores begins to evaporate (starting with the largest sized pore first (lowest energy)) according to the ambient humidity. Capillary stresses induced by drying shrinkage are dictated by the ambient RH according to Kelvin's equation (equation 2-1) (Adamson and Gast, 1997). This loss of moisture creates large capillary stresses that shrink the concrete. Capillary stresses (P_{cap}) can be used to calculate the ultimate paste shrinkage using the Mackenzie-Bentz equation (equation 2-2) (Bentz et al. 1998, Mackenzie 1950).

$$P_{cap} = \frac{RT \ln\left(\frac{\mathrm{RH}}{\mathrm{x_w}}\right)}{V_m} \tag{2-1}$$

Where

RH = Ambient relative humidity (%)

R = Universal gas constant

T = Absolute temperature

V_m = Molar volume of pore solution

x_w = (mol water/mol pore solution)

$$\varepsilon_p = \frac{S}{3} P_{cap} \left(\frac{1}{K} - \frac{1}{K_S}\right) \tag{2-2}$$

Where

P_{cap} = Capillary stresses

S = Volumetric degree of saturation

K = Bulk modulus

K_s = Bulk modulus of solid skeleton (e.g. C-S-H or C-A-S-H)

The other key factor in drying shrinkage involves the carbonation and decalcification of C-S-H gel. Carbonation of concrete starts with the chemical reaction between carbon dioxide (CO_2) in the atmosphere and the pore solution of concrete. This reaction results in the formation of carbonic acid ($CaCO_3$) (equation 2-3) (Mindess et al., 2003). Subsequently, the carbonic acid reacts with the calcium bearing phases in cement paste (specifically, C-S-H and CH) amd decreases the calcium content. Typically, carbonation of cement paste decreases the pH of the concretes solution (pH<9); however, when CH is carbonated, the deposition of Ca^{2+} ions into the pore solution "buffers" the solutions pH and mitigates further carbonation of the vital C-S-H gel (Neville, 2006). If, however, carbonation of C-S-H does occur, the carbonic acid attacks the gel as it decomposes into a much softer silica gel that is prone to significant drying shrinkage (equation 2-4) (Puertas et al. 2006).

$$Ca(OH)_2 + CO_2 = CaCO_3 + H_2O \tag{2-3}$$

$$C-S-H + C^* \rightarrow C-S-H + CC^* + H \tag{2-4}$$

One factor governing the rate of carbonation is the concretes internal relative humidity (other parameters include w/c and permeability). At a high humidity, CO_2 cannot easily penetrate the concrete because the coefficient of permeability of the water filled pores is very low (Neville, 2006); therefore, carbonation is essentially nonexistent during moist curing (100% RH). However, after moist curing has ended, the concrete loses some moisture according to the ambient relative humidity. This dramatically increases the rate of carbonation as CO_2 can then easily penetrate the air filled pores of the concrete. However, Verbeck (1958) has shown (Figure 2-8) that the rate of carbonation is highest at 50% RH and decreases as the humidity approaches 30%. Neville (2006) suggests that this is due to the significant loss of moisture at very low

humidities, where the moisture content of the concrete is so low that CO_2 cannot react to form the carbonic acid needed for carbonation to occur.

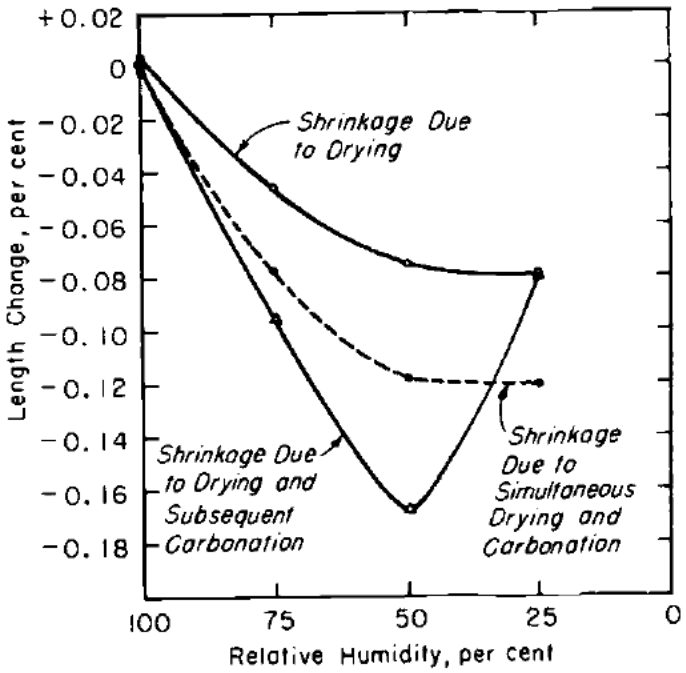

Figure 2-8: Drying and carbonation shrinkage in a concrete sample. Source: Verbeck (1958)

The combination of moisture loss and carbonation accounts for the total drying shrinkage in concrete. Carbonation of C-S-H paste creates a softer material (silica gel), which at a specific relative humidity, shrinks more than an equivalent paste that has not undergone carbonation. Figure 2-8 displays this phenomenon. Concrete that has experienced both carbonation and moisture loss experiences the most drying shrinkage. The drying shrinkage due to the combination of moisture loss and carbonation can be twice as high as the drying shrinkage solely due to moisture loss (Hewlett 1998). It is important to quantify both types of shrinkage to determine each type's contribution to total drying shrinkage. Measuring drying shrinkage under nitrogen (N_2) purge in a controlled environment eliminates the effects of carbonation; therefore,

only shrinkage due to moisture loss is measured. Measuring drying shrinkage under N_2 purge will help determine which shrinkage mechanism (carbonation or moisture loss) dictates total drying shrinkage in AAS pastes.

Many researchers (Shi et al. 2006, Melo Neto et al. 2008, Douglas et al. 1992, Bakharev et al. 2000, Palacios and Puertas 2007, Cincotto et al. 2003) have shown that alkali-activated slag (AAS) concrete has significantly higher drying shrinkage strains than ordinary Portland cement (OPC) mixtures. Palacios and Puertas (2007) measured drying shrinkage of mortar for OPC and AAS activated by an aqueous sodium silicate solution. Figure 2-9 shows that drying shrinkage of the AAS was approximately four times larger than the OPC.

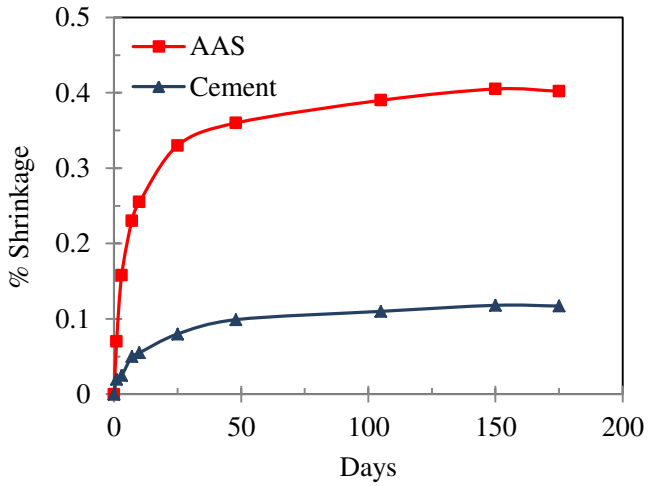

Figure 2-9: Drying shrinkage measurements of AAS and OPC mortars. Source: Palacios and Puertas 2007

2.10.2 Autogenous Shrinkage

A unique occurrence during concrete maturation is the tendency of the paste to shrink even in sealed systems where carbonation and moisture loss are nonexistent. Also known as self-desiccation, this autogenous shrinkage occurs as a result of chemical shrinkage. As cementitious materials begin to hydrate, a reduction in volume (chemical shrinkage) occurs because the

volume of the hydration products (i.e., cement paste) is smaller than the volume of reactants (i.e., water and cement). When the paste is still in its plastic state (before the final time of set), it cannot resist this reduction in volume and collapses inward on itself. This is seen as an apparent volume reduction; however, once it gains enough strength to form a solid skeleton, the paste can resist the chemical shrinkage deformations as air voids begin to form due to the continuous chemical hydration and shrinkage of the cementitious material. This occurrence is depicted in Figure 2-10. As the paste continues to hydrate and consume water, tiny menisci appear in the pores of the paste. The hardened, porous skeleton then begins to experience autogenous shrinkage as the surface tension of the pore solution creates large capillary stresses that pull on the pore walls of the concrete. This phenomenon can be described using the Laplace equation (equation 2-5). Similarly, capillary stresses can then be converted to ultimate shrinkage of the paste using the Mackenzie-Bentz equation (equation 3-3) (Bentz et al. 1998, Mackenzie 1950).

$$P_{cap} = -\frac{2\gamma cos\theta}{r} \tag{2-5}$$

Where

P_{cap} = Magnitude of capillary stresses

γ = Surface tension of pore solution

θ = Solid-solution contact angle

r = Radius of the largest pore emptied

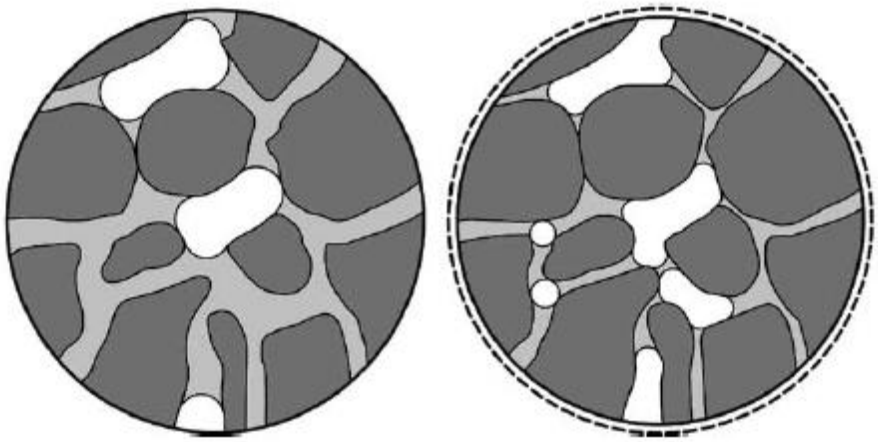

Figure 2-10: Left: Early age cement undergoing hydration. Right: A more mature cement with increasing air void formations. Source: Jensen and Hansen (2001)

AAS autogenous shrinkage strains have been reported (Bakharev et al. 1999, Cincotto et al 2003, Chen et al. 2007, and Collins et al. 2000) to be up to seven times higher than OPC. Figure 2-11 displays the autogenous shrinkage measurements of various AAS mixtures measured by Melo Neto et al. (2008). From this graph, it's easy to conclude that (1) AAS autogenous shrinkage strains are very large (as high as 2500 microstrains) and (2) AAS shrinkage strains vary significantly depending on the activating solution.

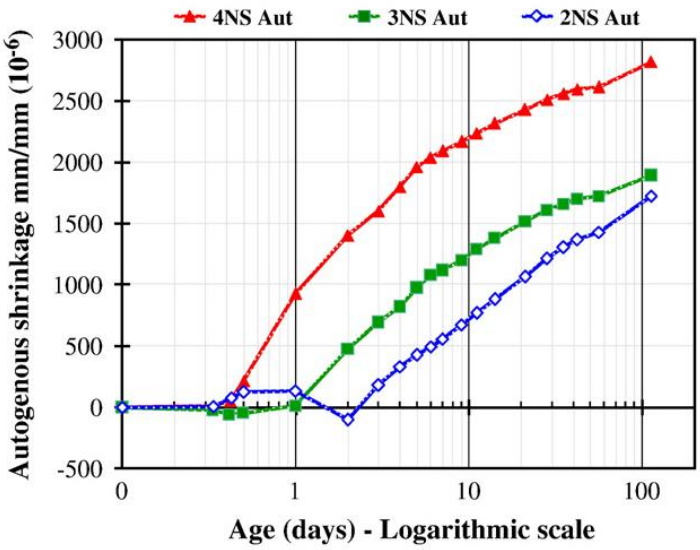

Figure 2-11: Autogenous shrinkage measurements of AAS mortar. Source: Melo Neto et al. (2008)

2.11 Effect of Activator Type and Dosage on AAS Properties

It can be reasonably expected that adjusting the activator type and dosage will affect the properties and characteristics of AAS systems. The water-glass modulus, shown in equation 2-6, can be used to characterize the silica to sodium oxide ratio of this activator. Krizan and Zivanovic (2002) performed research on AAS activated by various dosages of sodium silicate and sodium hydroxide to determine the effect of the activator modulus on compressive strength and drying shrinkage. They found that every AAS mixture had higher compressive strengths than the corresponding OPC, yet most AAS systems had larger drying shrinkage strains than the corresponding OPC.

$$n = \frac{SiO_2}{Na_2O} \tag{2-6}$$

Where

n = Activator modulus

SiO_2 = Silica concentration [M]

Na_2O = Sodium concentration [M]

It was shown (Krizan and Zivanovic (2002)) that among AAS systems, increasing the activator modulus while maintaining a constant sodium concentration increased the compressive strength but also increased the drying shrinkage. For example, when the activator modulus was doubled from 0.6 to 1.2, Krizan and Kivanovic (2002) saw a 133% increase in drying shrinkage but only a 25% increase in compressive strength. When the modulus was held constant and activator dosage was increased, similar results were observed. In general, an increase in activator modulus and/or dosage increases the AAS compressive strength as well as the drying shrinkage (Krizan and Kivanovic (2002))

Similar results are seen in autogenous shrinkage measurements. Melo Neto et al. (2008) tested three AAS systems with different activator concentrations (mixtures were named 2NS, 3NS, and 4NS). Each mixture was activated by a water glass solution with a modulus of 1.7; however, different activator concentrations were used (4NS had the largest while 2NS had the smallest). It was found mixture 4NS shrank significantly more than the other two. In general, a higher activator dosage results in larger autogenous shrinkage strains (Figure 2-11).

2.12 Shrinkage Mechanisms

Many researchers have attempted to explain this high autogenous shrinkage by linking it to a small pore size distribution. A fine pore structure will create very large capillary and autogenous stresses. It has been shown that AAS pastes have a very different pore size distribution compared to OPC. OPC pastes have a large percentage of micropores (<1.25nm) and macropores (25-5000 nm), whereas AAS pastes have a large percentage of mesopores (1.25-

25nm) (Collins et al. 2000). Ben Haha et al. (2011) found that waterglass activated systems have smaller pores than NaOH activated systems, most likely due to the slower hydration of water-glass AAS and the existing aqueous silica in the solution which can react with dissolved Ca^{2+} from slag to form C-S-H not only at the surface of slag particles but also in the space in between the particles (Fig. 2-6).

Chemical shrinkage is the driving force behind autogenous shrinkage (Tazawa et al. 1995). No experimentally measured chemical shrinkage data for AAS systems are available in the literature; however, Thomas et al. (2012) has modeled and estimated a theoretical maximum value of chemical shrinkage for AAS between 11.5 to 13.9 ml/100g of slag reacted. This is much higher than the well-known chemical shrinkage of Portland cement (6.4ml/100g cement) (Powers et al. 1948, Jensen et al. 2001) and would help explain the large autogenous strains of AAS. However, the maximum theoretical chemical shrinkage value assumes all the slag has reacted. It has been shown (Ben Haha et al. 2011) that AAS pastes have a relatively low degree of hydration (about 40%) compared to OPC. As such, chemical shrinkage measurements need to be adjusted for the degree of hydration.

2.13 Carbonation

Vulnerability to carbonation is also a reasonable explanation for these large deformations. Carbonation in cementitious materials occurs when CO_2 dissolves in pore solution and forms carbonic acid; this acid then attacks the calcium bearing phases present in the concrete (Siddique and Khan 2011, Bakharev et al. 2001). Decalcification, the loss of calcium through chemical reaction, occurs to both calcium hydroxide (CH) and the C-S-H gel in concrete (Chen et al. 2006). As the carbonic acid attacks cement paste, carbonated C-S-H decomposes into a much

softer silica gel with large drying shrinkage strains (Chen et al. 2006). A detailed discussion on the mechanisms of carbonation and carbonation shrinkage can be found in section 3.2.7.

Many scientists (Puertas et al. (2006), Siddique and Khan (2011)) have shown that alkali-activated slag cements experience intense carbonation rates (up to 200% higher than Portland cement). As suggested by Shi et al. (2006), high carbonation in AAS is probably due to the limited formation of solid CH and the low calcium to silica ratio (C/S) of C-S-H. Decalcification of C-S-H gel only occurs when solid CH is inaccessible or locally depleted (Taylor 1997); therefore, the limited presence of CH in AAS cements does not mitigate carbonation of C-S-H as it does in OPC cements.

Bakharev et al. (2001) have shown that after one year of CO_2 exposure, the depth of carbonation in AAS concretes (20 mm) was almost twice as large as it was in OPC concretes (12mm). Additionally, after experiencing carbonation, AAS concretes have shown (Bakharev et al. 2001) to have compressive strength reductions while some OPC concretes actually gained strength after carbonation. No data is available to determine how much of the resulting drying shrinkage is due to carbonation and how much is caused by loss of moisture.

2.14 Shrinkage Mitigation

While many researchers have attempted to mitigate shrinkage in AAS concrete, none have found complete success, mainly due to lack of knowledge of mechanisms governing AAS shrinkage. Palacios and Puertas (2007) attempted to reduce the shrinkage in AAS using shrinkage reducing admixtures (SRAs). SRAs are beneficial due to the reduction in surface tension of the pore solution (Radlinska et al. 2007). Palacios and Puertas (2007) reported reductions in autogenous and drying shrinkage strains; however, drying shrinkage strains remained significantly higher than those of OPC systems.

Similarly, Collins et al. (2000) attempted to use known mitigation strategies to solve the shrinkage problem in AAS. Presoaked porous coarse aggregates were used to create an internal reservoir of curing water that can further hydrate the cementitious material. They found that this reduced the autogenous strains of AAS systems, but the porous aggregates eventually lost all moisture to ambience under drying conditions. Therefore, use of coarse aggregates in internal curing simply delays and does not prevent drying shrinkage (Radlinska et al. 2007). Other scientists (Sakulich and Bentz, 2012) have recently attempted to eliminate autogenous shrinkage in AAS cements; however, chemical shrinkage was not properly measured and LWA proportioning was calculated incorrectly. The use of a properly proportioned lightweight fine aggregate can be used to completely eliminate autogenous shrinkage. A proper sized aggregate is crucial to the success of this mitigation strategy due to the low permeability of the AAS pastes (Bentz et al., 1999).

2.15 Literature Conclusions

While limited data related to shrinkage performance of AAS do exist, the scientific reasoning and mechanisms of large shrinkage in AAS have not been explained. A comprehensive study that investigates all potential shrinkage mechanisms has not been performed. Further research is needed to properly quantify different forms of shrinkage (e.g., chemical, autogenous, drying, carbonation), and to present and evaluate hypotheses explaining why AAS undergoes a large shrinkage and shows a higher risk of cracking. Bridging such knowledge gaps will result in developing efficient shrinkage mitigation tools for alkali-activated concretes.

2.16 References

Adamson, A.W., Gast, A.P. (1997) *Physical Chemistry of Surfaces, 6th Ed.*, Wiley-Interscience, New York.

American Society of Civil Engineers (ASCE), 2013, http://www.infrastructurereportcard.org (accessed May 20, 2013).

Bakharev, T., Sanjayan, J.G., Chen, Y.B. (1999), "Alkali activation of Australian slag cements", Cement and Concrete Research, 29, 112-120.

Bakharev, T., Sanjayan, J.G., Cheng, Y.B. (2000), "Effect of admixtures on properties of alkali-activated slag concrete." Cement and Concrete Research, 30, 1367-1374.

Bakharev, T., Sanjayan, J.G., Chen, Y.B. (2001), "Resistance of alkali-activated slag concrete to carbonation. Cement and Concrete Research, 1277-1283.

Ben Haha, M., Le Saout, G., Winnefeld, F., Lothenbach, B. (2011), Influence of activator type on hydration kinetics, hydrate assemblage and microstructural development of alkali activated blast furnace-slags. Cement and Concrete Research, 41 301-310.

Bentz, D.P., Garboczi, E.J., Quenard, D.A. (1998) Modeling drying shrinkage in reconstructed porous materials: Application to porous Vycor glass. Modeling and Simulation in Materials Science and Engineering, 6, 211-236

Bentz, D.P., Snyder, K.A. (1999), "Protected paste volume in concrete: Extension to internal curing using saturated lightweight fine aggregate", Cement and Concrete Research, 29, 1863-1867.

Brough, A.R., Atkinson, A. (2002), Sodium silicate-based, alkali-activated slag mortars Part I. Strength, hydration, and microstructure. Cement and Concrete Research 32, 865-879.

Chang, J.J. (2003), A study on the setting characteristics of sodium silicate-activated slag pastes, Cement and Concrete Research, 22, 1005-1011

Chen, J.J., Thomas, J.J., Jennings, H.M. (2006), Decalcification shrinkage of cement paste, Cement and Concrete Research, 36, 801-809

Chen, W., Brouwers, H.J.H. (2007), "The hydration of slag, part 1: reaction models for alkali-activated slag." J Mater Sci, 42:428-443.

Cincotto, M.A, Melo A. A., Repette, W.L. (2003), "Effect of different activators type and dosages and relation to autogenous shrinkage of activated blast furnace slag cement." In: G. Grieve, G. Owens, Eds, Proc. 11th International Congress on the Chemistry of Cement, Durban, South Africa, (2003) 1878-1888.

Collins, F.G., Sanjayan, J.G. (1999), "Workability and mechanical properties of alkali activated slag concrete". Cement and Concrete Research, 29, 455-458.

Collins, F.G., Sanjayan, J.G. (2000), Effect of pore size distribution on drying shrinkage of alkali-activated slag concrete. Cement and Concrete Research, 30 1401-1406.

Damtoft, J.S., Lukasik, J., Herfort, D., Sorrentino, D., Gartner, E.M. (2008), Sustainable development and climate change initiatives, Cement and Concrete Research, 38, 115-12.

Davidovits, J. (1994), "Properties of geopolymer cements", 1st International Conference on Alkaline Cements and Concretes, Kiev, Ukraine, 1, 131-149.

Douglas, E., Bilodeau, A., Malhotra, V.M. (1992), Properties and durability of alkali-activated slag concrete, ACI Materials Journal, 89, 509-516.

Fernandez-Jimenez, A., Palomo, J.G., Puertas, F. (1999), "Alkali-activated slag mortars Mechanical strength behavior", Cement and Concrete Research, 29, 1313-1321.

Flavin, C., Tunali, O. (1996), Climate of Hope: New Strategies for Stabilizing the World's Atmosphere, Paper No. 130, Worldwatch Institute, Washington D.C., 84pp.

Hewlett, P (1998), Lea's Chemistry of Cement and Concrete, Elsevier Ltd., Burlington, MA

Intergovernmental Panel on Climate Change (IPCC) (2001), Climate Change 2001: The Scientific Basis, Cambridge University Press.

hydrate", Journal of the American Ceramic Society, 69, 614-418.

Jensen, O.M., Hansen, P.F. (2001) "Water-entrained cement-based materials: Principles and theoretical background." Cement and Concrete Research, 31, 647-654.

Jolicoeur, C., Simard, M.A.m Sharman, J., Zamojska, R., Dupuis, M., Spiratos, N., Douglas, E., Malhotra, V.M. (1992), "Chemical activation of blast-furnace slag, An overview and systematic experimental investigation", Advances in Concrete Technology, Ministry of Supply and Services, Ottowa, Canada, 471-502.

Krizan, D., Zivanovic, B. (2002), Effects of dosage and modulus of water glass on early hydration of alkali-slag cements, Cement and Concrete Research, 32, 1181-1188.

Luke, K., Glasser, F.P. (1987), Selective dissolution of hydrated blast furnace slag cements, Cement and Concrete Research, Vol. 17, pp. 273-282.

Mackenzie, J.K. (1950) "The elastic constants of a solid containing spherical holes." Proceedings of the Physical Society, 683, 2-11.

Marinshaw, R., Wallace, D., (1994). "Emission factor documentation: Portland cement manufacturing." United States Environmental Protection Agency (EPA), www.epa.gov/ttn/chief/ap42/ch11/bgdocs/b11s06.pdf (accessed May 15, 2013).

Mehta, K. (2002), Greening of the Concrete Industry for Sustainable Development, Concrete International.

Melo Neto, A.A, Cincotto, M.A., Repette, W. (2008) "Drying and autogenous shrinkage of pastes and mortars with activated slag cement." Cement and Concrete Research 38(4) 565-574.

Mindess, S., Young, J.F., Darwin, D. (2003), Concrete 2nd Ed., Prentice Hall, Upper Saddle River, New Jersey.

National Slag Association (2009), http://www.nationalslag.org/blastfurnace.htm, accessed May 20, 2013.

Neville, A.M. (2006), *Properties of Concrete 4th Ed.*, Pearson Education Limited, London, England.

Pal, S.C., Mukherjee, A., Pathak, S.R. (2003), "Investigation of hydraulic activity of ground granulated blast furnace slag in concrete," Cement and Concrete Research, 33, 1481-1486.

Palacios, M., Puertas, F. (2007), Effect of shrinkage-reducing admixtures on the properties of alkali-activated slag mortars and pastes, Cement and Concrete Research 37, 691–702.

Paul, A. (1990), Chemistry of Glasses 2nd Ed., Chapman and Hall, New York, New York.

Powers, T.C., Brownyard, T.L. (1948) "Studies of the physical properties of hardened portland cement paste." Bulletin 22, Research Laboratories of the Portland Cement Association, Chicago.

Puertas, F., Palacios, M., Vazquez, T. (2006) "Carbonation process of alkali-activated slag mortars", Journal of Materials Science, 41, 3071-3082.

Radlinska, A., Rajabipour, F., Bucher, B., Henkensiefken, R., Sant, G., Weiss, J. (2007), Shrinkage Mitigation Strategies in Cementitious Systems: a Closer Look at Differences in Sealed and Unsealed Behavior, Transportation Research Board.

Radlinska, A., Salera, M., Ernst, S., Yost, J., Rajabipour, F. (2012), "Linking material and structural response of alkali-activated fly ash binders." International Congress on Durability of Concrete.

Ravukimar, D, Peethamparan, S, Neithalath, N (2010), Structure and strength of NaOH activated concretes containing fly ash or GGBFS as the sole binder, Cement and Concrete Composites, 32, 399-410.

Sakulich, A.R., Bentz, D.P. (2012), "Mitigation of autogenous shrinkage in alkali activated slag mortars by internal curing", Materials and Structures, RILEM.

Sant, G., Lura, P., Weiss, J. (2005), Measurement of Volume Change in Cementitious Materials at Early Ages, Transportation Research Board.

Shelby, J.E. (2005), Introduction to Glass Science and Technology, The Royal Society of Chemistry, Cambridge CB4 0WF, UK.

Shi, C., Krivenko, P., Roy, D. (2006), Alkali-Activated Cements and Concrete, Taylor & Francis.

Shi, C, (2003) "Corrosion resistance of alkali-activated slag cement", Advances in Cement Research, 15 (2), 77-81.

Siddique, R., Iqbal Khan (2011), M. Supplementary Cementing Materials. Chapter 3: Ground Granulated Blast Furnace Slag. Engineering Materials, DOI. Springer-Verlag Berlin Heidelberg 2011.

Taylor, H.F.W. (1997), Cement Chemistry 2nd Edition, Thomas Telford, London.

Tazawa, E., Miyazawa, S., Kasai, T. (1995), "Chemical shrinkage and autogenous shrinkage of hydrating cement paste", Cement and Concrete Research, Vol. 25, No.2, pp. 288-292.

Thomas, J.J., Allen, A.J., Jennings, H.M. (2012) "Density and water content of nanoscale solid C-S-H formed in alkali-activated slag (AAS) paste and implications for chemical shrinkage." Cement and Concrete Research, 42, 377-383.

Verbeck, G.J. (1958), "Carbonation of hydrated Portland cement", *ASTM Sp. Tech. Publ. No.* 205, pp. 17-36.

Wang, S., Schrivener, K., Pratt, P. (1994), Factors affecting the strength of alkali-activated slag. Cement and Concrete Research, Vol. 24, No. 6, pp. 1033-1043.

Wang, S., Pu, X, Scrivener, K.L., Pratt, P.L., (1995), "Alkali activated slag cement and concrete: A review of properties and problems", Advances in Cement Research, 7, 93-102.

Wang, S. (2000), The role of sodium during the hydration of alkali-activated slag, Advances in Cement Research, 12, No. 2, Apr., 65-69.

Wu, C., Zhang, Y., and Hu, Z., (1993), “Properties and application of alkali-slag cement”, Journal of the Chinese Ceramic Society, 21 (2), 176-181.

Chapter 3

Shrinkage characteristics of alkali-activated slag cements

Christopher Cartwright; Farshad Rajabipour; Aleksandra Radlińska

Manuscript accepted and published by ASCE Journal of Materials in Civil Engineering

ABSTRACT: Recent interest in creating green construction materials has sparked the development of portland cement-free binders. Alkali-activated slag (AAS) concrete has a low embodied energy and comparable or superior strengths to ordinary portland cement (OPC) concrete. However, one factor limiting the AAS usage is its durability performance, specifically its susceptibility to shrinkage. Before declaring AAS a marketable product, the mechanisms behind its volumetric instability need to be understood. This paper presents a preliminary study of the shrinkage deformations of various AAS mixtures, where four unique AAS mortars were designed and tested for autogenous, chemical, and drying shrinkage, time of setting, and compressive strength. All results were compared to those obtained for a control OPC mortar. It was found that AAS mixtures, with comparable strength to OPC, show a higher autogenous and drying shrinkage. A lower elastic stiffness, higher degree of saturation, and potentially higher chemical shrinkage contribute to the high autogenous shrinkage of AAS. A lower elastic stiffness also leads to a large drying shrinkage, although other mechanisms, such as reduced pore size and carbonation shrinkage, are likely to also contribute to the high drying shrinkage measured for AAS.

3.1 Introduction

Concrete production utilizes the most abundant natural materials present on the Earth's surface. However, the high temperatures (up to 1500°C) required during production of portland cement in the kiln result in a significant energy use (embodied energy ≈ 5.7MJ/kg of cement) and a large CO_2 footprint (approximately 0.95kg CO_2/kg of cement) (Ashby, 2009). Altogether, cement production is responsible for approximately 5% of the total anthropogenic GHG emissions (Damtoft et al., 2008) – roughly equivalent to the CO_2 output of the entire nation of Japan. This raises sustainability concerns and fosters significant interest in portland cement-free binders.

Multiple environmentally friendly products have been researched up to date to partially or fully replace portland cement in concrete. Research has shown (Ben Haha et al., 2011, Shi et al., 2006) that industrial waste products, e.g. blast furnace slag from steel manufacturing, can be used to successfully produce a portland cement-free concrete when activated by an alkaline solution. Ground granulated blast furnace slag (GGBFS) is an amorphous material mainly comprised of calcium and alumino-silicates (Shi et al., 2006). Alkali activation is the process of exposing these glassy materials to a high pH environment to accelerate the congruent dissolution of alumino-silicates. The dissolved products can then react with water and the available alkali and calcium ions to form calcium silicate hydrate (C-S-H) and calcium-alumino-silicate hydrate (C-A-S-H) products that provide the binder phase in concrete (Ben Haha et al., 2011). The process of alkali activation of these amorphous materials allows for the development of a portland cement-free binder.

Alkali-activated concretes (AAC) can offer superior properties over ordinary portland cement (OPC) concrete, including potential for very high compressive strength (up to 130 MPa) and excellent performance against fire and chemical (acid, sulfate) attack (Shi et al., 2006). A

recent environmental life-cycle assessment (LCA) study shows that alkali-activated slag (AAS) concrete has 73% lower greenhouse gas (GHG) emissions, 43% less embodied energy, 25% less water use, and 22 to 94% lower values of different environmental toxicity impact parameters, in comparison with OPC concrete of similar compressive strength (Jiang et al., 2014). Despite their favorable performance, the marketability and acceptance of alkali-activated concretes in the industry have been hindered partly by concerns related to their long-term durability. Perhaps one of the most significant conundrums impeding the implementation of AAC is their volumetric instability. For example, Shi et al. (2006) has shown that AAS concrete has significantly higher shrinkage than OPC. Palacios and Puertas (2007) measured drying shrinkage of mortar for OPC and AAS activated by an aqueous sodium silicate solution. It can be seen (Figure 3-1) that shrinkage of the AAS was approximately four times larger than the OPC. While limited data related to shrinkage performance of AAS do exist (Shi et al., 2006, Melo Neto et al., 2008, Douglas et al., 1992, Bakharev et al., 2000, Palacios and Puertas, 2007, Cincotto et al., 2003), the scientific reasoning and mechanisms of large shrinkage deformations in AAS have not been explained. For instance, some researchers (Collins and Sanjayan, 2000, Palacios and Puertas, 2007) suggest that a refined pore structure creates large autogenous strains that play a significant role in the shrinkage of AAS systems; however, a comprehensive study that investigates all potential shrinkage mechanisms has not been performed. Further research is needed to properly quantify different forms of shrinkage (e.g., chemical, autogenous, drying and carbonation) and to present and evaluate hypotheses explaining why AAS undergoes a large shrinkage and shows a higher risk of cracking. This paper presents the preliminary results of a research aimed at addressing the aforementioned objectives. It provides the results for the development of several AAS mortar mixtures and characterizes their susceptibility to different forms of shrinkage.

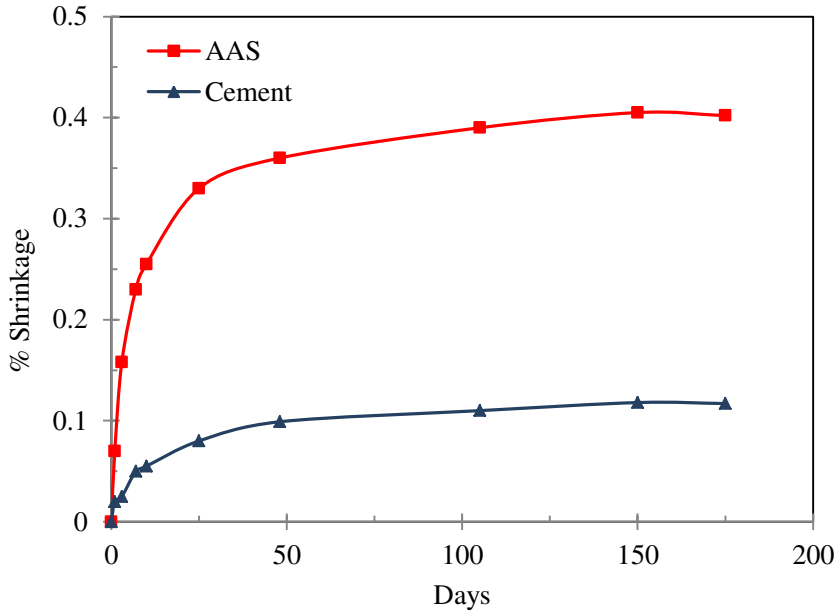

Figure 3-1. Drying shrinkage measurements of AAS mortar compared to OPC mortar (reproduced using data from Palacios and Puertas (2007))

3.2 Materials

Alkali-activated slag paste and mortar mixtures were investigated in this study. The grade 120 (ASTM C989M-12a) ground granulated blast-furnace slag was used that had a density of 2.89 g/cm^3, and an oxide composition as shown in Table 3-1. A particle size analysis (using laser diffraction) showed that 50% of slag particles were smaller than 7.4μm and 10% of slag particles were smaller than 1μm (Figure 3-2). Portland cement was ASTM C150 type I cement with a density of 3.14 g/cm^3 and an oxide composition as shown in Table 3-1. A quantitative analysis on XRD of slag powder was performed and found a mainly amorphous material with trace amounts of crystalline calcium sulfate ($CaSO_4$) and tri-calcium silicate (Ca_3SiO_5).

Table 3-1. Oxide compositions of slag and portland cement (mass %)

	CaO	SiO_2	Al_2O_3	MgO	SO_3	Fe_2O_3	Na_2O	K_2O	LOI
Slag (GGBFS)	47.5	30.8	11.45	3.65	3.03	1.81	0.17	0.38	1.17
Type I cement	62.5	19.9	5.44	2.31	4.93	2.26	0.30	0.89	0.86

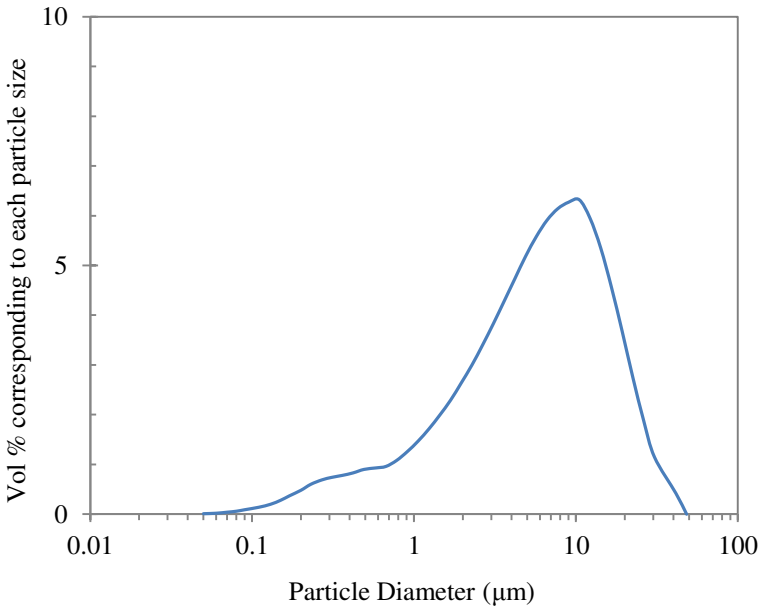

Figure 3-2. Particle size distribution of slag powder

Four AAS mortars and a control OPC mortar were designed using a constant volumetric liquid (water + activator) to solid (slag or cement) ratio of 1.30, yielding an initial binder porosity of 56.5% in all five mixtures. For the control OPC mixture, this is equivalent to a mass-based w/c = 0.414. For the AAS mixtures, the mass-based liquid to solid ratio was in the range 0.489 to 0.510, depending on the concentration and density of the activating solutions (Tables 3-2 and 3-3). The aforementioned liquid to binder ratios are based on saturated surface dry (SSD) condition of aggregates; i.e., they do not account for any aggregate absorption. For all mixtures, a natural river sand, meeting ASTM C33M-11a requirements, was used. The sand had a fineness modulus 2.60, oven dry specific gravity 2.52, and absorption capacity 2.0%. Each mortar mixture was designed with a 50.7% volume fraction of sand. The mixture proportions of the mortars are listed in Table 3-2.

Table 3-2. Mortar mixture proportions (per liter of mortar)

Mix ID (*Description*)	NaOH (g)	$Na_2O(SiO_2)_n$ (g)	Water* (g)	Portland Cem (g)	Slag (g)	O.D. Sand (g)
Control (*OPC mortar*)	0	0	296.8	656.6	0	1,247
AAS1 (*Lower SiO_2 Na-Si*)	23.77	35.70	263.6	0	603.9	
AAS2 (*Higher SiO_2 Na-Si*)	5.94	95.49	234.6			
AAS3 (*2M NaOH*)	23.77	0	285.9			
AAS4 (*4M NaOH*)	47.54		274.8			

*Note: Water content includes absorption by oven dry sand

Mortars AAS1 (lower silica concentration) and AAS2 (higher silica concentration) were activated using an alkaline solution which contained a combination of dissolved sodium hydroxide (NaOH) pellets, aqueous sodium silicate (Na2O(SiO2)n) (also known as waterglass), and water. The other two mortars, AAS3 and AAS4, were activated using only a solution of NaOH in water (either 2M or 4M). The aqueous sodium silicate ((Na2O(SiO2)n) had the modulus n = 1.60, pH = 13.7, and specific gravity = 1.60 at 20°C. It contained 53.2% water, 28.8% SiO2, and 18.0% Na2O by mass. To prepare the activating solutions, reagent sodium hydroxide pellets were first dissolved in water at room temperature while covered to prevent carbonation. The solution was shaken for 5 minutes and then set aside for approximately two hours to allow for dissipation of the heat of dissolution and a return to room temperature. For mortars AAS1 and AAS2, the sodium hydroxide and sodium silicate solutions were kept separate. The sodium hydroxide solution, sand, and slag were added to the mixing bowl and mixed according to ASTM C305-12. In order to allow the solution to properly dissolve the slag, the sodium silicate was excluded from the mixture until 15 minutes after mixing. The sand was oven dried but cooled in advance to room temperature. The mortar proportions reported in Table 3-2 account for the absorption of water (or the activating solution) by the sand. It is worth mentioning that preparation of the liquid phase of AAS (a solution of alkaline activators in water) is clearly a

more involved process than the liquid phase in OPC concrete, being tap water. This poses a challenge in adopting AAS as a viable and practical alternative to OPC concrete in the construction industry. However, research is currently ongoing to address this issue, for example by blending the powder form of activators to slag, so only water has to be added at the ready mixed plant (Ravikumar and Neithalath, 2012). Alternatively, AAS liquid phase could be prepared in advanced or sold in a concentrated or ready to use form, similar to the current practice for chemical admixtures.

To ensure similar consistency among the five mortar mixtures, the flow test (ASTM C1437-07) was performed on the fresh mortars after mixing, and a small dosage of water reducing admixture was added to each mixture, as needed to achieve a similar flow of 100%. Individual WRA dosages per mixture can be found in Table 3-3. For mortars AAS1 and AAS2, the entire WRA dosage was added to the sodium hydroxide solution before adding the sodium silicate solution.

Table 3-3. Activating solution properties for AAS mixtures

Mix ID	$n = (SiO_2/Na_2O)$ molar-based	pH	Density (g/cc)	WRA (mL/kg_{slag})
AAS1	0.41	14.31	1.09	5.00
AAS2	1.22	13.78	1.13	2.00
AAS3	0	14.30	1.04	4.15
AAS4	0	14.60	1.09	8.00

3.3 Experimental Methods

All mortars were mixed according to ASTM C305-12. The correct dosage of WRA was added to the activating solution (NaOH portion) before mixing. Once all ingredients were ready for mixing, the activating solution, slag, and sand were poured into an electric (Hobart) mixer and mixed at slow speed (140 ± 5 rev/min) and medium speed (285 ± 5 rev/min) according to ASTM C305-12.

To evaluate the workability and flow of mortar mixtures, the procedure listed in ASTM C1437-07 was used. After the fresh mortar was mixed, it was placed in a flow mold on a drop table. The diameter of the new shape of the mortar after testing was measured at four locations using a calliper. The percent flow was calculated using the measured diameter after the test and the original diameter of the flow mold (10.16 cm).

Initial and final setting times of mortars were measured according to ASTM C403M-08. Each mortar mixture was mixed and placed in a cylindrical mold: 15.24 cm in diameter and 15.24 cm in height. The mold was moist cured (100% RH, 23±0.5°C) for the entirety of the test. A spring reaction device was used for measuring penetration resistance of a needle at 30 minute intervals. The initial and final time of setting correspond (according to ASTM) to penetration resistances of 3.45MPa (500 psi) and 27.6MPa (4,000 psi), respectively.

Cubic specimens (50 × 50 × 50 mm) were prepared according to ASTM C109M-11b for compressive strength measurements. The mortar cubes were compacted using a vibrating table and a tamping rod. All mortar specimens were moist cured (100% RH, 23±0.5°C) until the time of testing. Using a standard compressive machine, cubes were loaded until failure at 1, 3, 7, and 28 days at a load rate of 345 kPa/s. For each mortar and at each age, 3 cubes were tested and the results were averaged.

The moisture content and porosity of the mortar mixtures were measured according to ASTM C642-13. Samples were mixed according to ASTM C305-12 and then either moist cured or sealed for 7 days. After 7 days, all samples were oven dried at 105°C until constant mass was achieved. The mortar was then submerged in water for 48 hours after which the samples were surface dried and mass was recorded. The samples were then placed in water and boiled for 5 hours; afterwards, they were surface dried and the mass was recorded. Finally, the samples were suspended by a wire in a water bath and their buoyant mass was measured.

The drying and autogenous shrinkage was tested using mortars, while the chemical shrinkage measurements were performed using paste samples of the same composition as the binder phase of the mortars. Drying shrinkage was measured using prism samples (2.54 × 2.54 × 25.4 cm). Fresh mortar was cast into prism molds and consolidated using a vibrating table and tamping rod. Prism bars were moist cured (100% RH, 23±0.5°C) for 7 days and then moved to a walk-in environmental chamber (50±3% RH, 23±0.5°C) to undergo drying. Length measurements were taken according to ASTM C490M-11, using a digital comparator with an accuracy of 0.0025 mm. Simultaneous mass measurements were taken to determine the moisture loss and degree of saturation. For each mortar, 4 prisms were tested and the results were averaged. The moisture content and porosity of duplicate mortar samples were measured at the end of moist curing (7 days) according to ASTM C642-13, as already mentioned.

Autogenous shrinkage of mortars was tested following the corrugated tube protocol (ASTM C1698-09). Four corrugated polyethylene cylindrical molds 2.9 cm in diameter and 42.0 cm in length were cast for each mixture (Figure 3-3). After mixing, the mortar was scooped into a funnel that was placed at the open end of the corrugated tube. After casting, the corrugated tubes were continuously rotated at a speed of 5 rev/min to prevent bleeding and segregation. The tubes were rotated until the first length measurement was taken at the final time of setting. Simultaneous mass measurements were made to ensure that the system was indeed sealed.

Duplicate specimens were used for measurement of moisture content and porosity at 7 days after casting, according to ASTM C642-13.

Figure 3-3. Corrugated polyethylene cylindrical molds for autogenous shrinkage measurement

Elastic modulus was measured at 28 days for all five mortar mixtures. The test was performed using two duplicate 100×200 mm cylinders per mixture. The mortar cylinders were demolded at 24 hours and moist cured until moments before testing at 28-days. Each cylinder was placed in a dual compressometer-extensometer, connected to a data acquisition system. This setup logged the longitudinal displacement readings through the use of LVDTs while the specimen was loaded in compression. The load rate used was 0.25±0.05 MPa/sec. This measurement takes into effect the elastic region from the 50 με point to 40% of the ultimate (failure) load for the age tested, otherwise known as the chord modulus. The LVDT readings were analyzed and converted to strains and compared against the applied stress to quantify the elastic modulus for the concrete.

Finally, chemical shrinkage was measured using the buoyancy method (Sant et al., 2005). When cementitious materials begin to hydrate, a reduction in volume occurs because the volume of the hydration products is generally smaller than the volume of reactants. This volumetric

change can be estimated by measuring the buoyancy of the hydrating paste during the first several days of hydration. Because the cementitious paste does not lose or gain mass in a sealed system, the only change in buoyancy force of the paste can be assumed to be due to the volume reduction caused by chemical shrinkage. After mixing slag powder with the activating solution, a 25g slag paste sample (5mm thick) was placed in a crystallizing dish (70 mm diameter × 50 mm height). A 10 mL solution, with the same composition of the activating solution, was placed on top of the sample. The dish was then filled with low density paraffin oil (0.863 g/cm^3). The sample was placed on a wire mesh and lowered into a stainless steel bucket filled with the oil. The bucket was placed in a water bath which was kept at constant temperature of 23±0.5°C. The wire mesh was attached to a string mounted to the underside of a high precision balance, capable of measuring mass with an accuracy of 0.0001g. The entire system was surrounded by a clear acrylic shield, to prevent wind currents from interfering with the mass measurements. Mass measurements were recorded every five minutes using an automatic data acquisition system. Chemical shrinkage was calculated using equation 3-1 (Sant et al., 2005) where $W_{sub}(30)$ is the submerged weight of the sample 30 minutes after mixing (considered as a reference point as suggested by Sant et al., 2005), $W_{sub}(t)$ is the submerged weight of the sample at any time t, ρ_{oil} is the density of the paraffin oil, and g_{slag} is the mass of slag in the paste sample.

$$V_{CS} = \frac{\Delta V_{paste}}{g_{slag}} = \frac{W_{sub}(t) - W_{sub}(30)}{\rho_{oil} * g_{slag}} \qquad (3\text{-}1)$$

3.4 Results

The measured initial and final time of setting of the four AAS mortar mixtures and the control OPC has been summarized in Table 3-4. Every AAS mixture except AAS3 has a shorter initial and final time of setting than the OPC. By comparing mixtures activated only by NaOH, it can be seen that AAS4 sets faster than AAS3, most likely due to the higher pH of AAS4, which results in a more accelerated dissolution of the slag powder. It is interesting to note that although AAS3 and AAS1 have a similar pH, AAS1 sets much quicker than AAS3. This is most likely due to the presence of aqueous silicates in AAS1 that contribute to rapid formation of C-S-H and C-A-S-H products. These results are consistent with other reports (Brough et al., 2002, Chang (2003)) on the time of setting of AAS mortars.

Table 3-4. Initial and final time of set of mortars

Mix ID	Initial Time of Set	Final Time of Set
AAS1	1 hour 25 minutes	2 hours 20 minutes
AAS2	4 hours 25 minutes	6 hours 25 minutes
AAS3	5 hours 45 minutes	8 hours 10 minutes
AAS4	3 hours 5 minutes	3 hours 55 minutes
OPC	5 hours 10 minutes	7 hours 15 minutes

Strength development for the four AAS mortar mixtures and the control OPC mixture has been summarized in Figure 3-4. It can be seen that two of the AAS mixtures (AAS2 and AAS4) have a compressive strength similar to or exceeding the OPC mortar. By comparing AAS1 and AAS2, it can be seen that although AAS2 has a lower pH and sets later than AAS1, it has a higher compressive strength at 1, 3, 7, and 28 days. This is likely due to a denser microstructure of the slag paste in AAS2 as a result of a higher concentration of admixed SiO_2. For mortars activated with NaOH only (AAS3 and AAS4), a higher pH results in a faster dissolution of slag and

therefore faster setting and higher strength. Additionally, although AAS1 and AAS3 have a similar pH, AAS1 has a higher compressive strength due to the addition of aqueous silicate that contributes to further formation of C-S-H and C-A-S-H. AAS3 shows the lowest strength among the five mortars, which could be an indication of the highest porosity and pore size. Our parallel study of the microstructure characterization of these mortars (to be published in a separate paper) confirms that among the four AAS mortars, AAS3 has the largest porosity and pore size measured by mercury porosimetry (MIP) and SEM imaging.

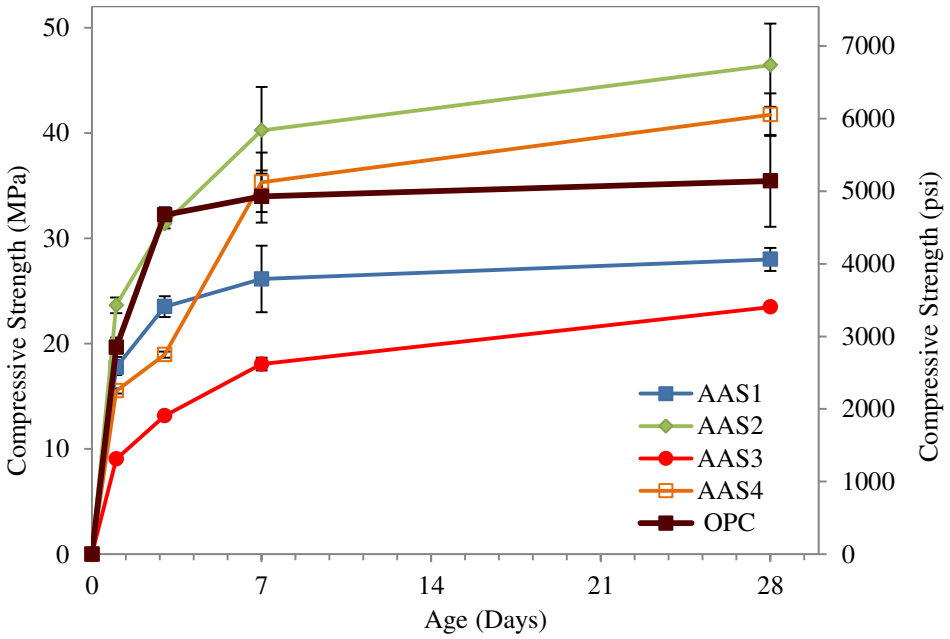

Figure 3-4. Compressive strength development for AAS and OPC mortars

The results for the 28-day static elastic modulus for all five mixtures are presented in Table 3-5. The results show that AAS3 and AAS4 have a smaller elastic modulus (approximately 13.5 GPa) than the other three mixtures (ranging from 19.49 to 20.71 GPa). AAS1, AAS2, and OPC show similar elastic modulus values at 28 days. Assuming a similar Poisson's ratio for all

mortars, it can be inferred that the bulk modulus (K as in equation 3-2) of mortars AAS3 and AAS4 is approximately 67% of that of the other three mortars.

Table 3-5. Modulus of elasticity of mortars at 28 days

Mix ID	Modulus of Elasticity (GPa)
AAS1	20.71
AAS2	19.85
AAS3	13.25
AAS4	13.55
OPC	19.49

Figures 3-5 and 3-6 show the results of drying shrinkage and the drying mass loss, respectively. During the 7 days of moist curing (23±0.5°C, 100%RH), the mortar bars gained weight (especially the OPC mortar) and showed a slight expansion of less than 60 με. With the start of drying, all mortars began to shrink considerably. The rate of shrinkage during the first week of drying was the highest for AAS2 (1335 με/wk) and lowest for AAS3 (332 με/wk). The OPC mortar shrank by 735 με/wk during the first week. Except AAS3, the long-term shrinkage strains of every AAS mixture exceeded that of the control OPC, which had an ultimate drying shrinkage of 1500 με after 178 days. Among the four AAS mixtures, AAS3 appears to show the smallest shrinkage, comparable with that of the OPC. The other three AAS mortars show comparable shrinkage magnitudes (3500 to 3800 με), which are approximately twice as large as the shrinkage of AAS3 and OPC (1650 με).

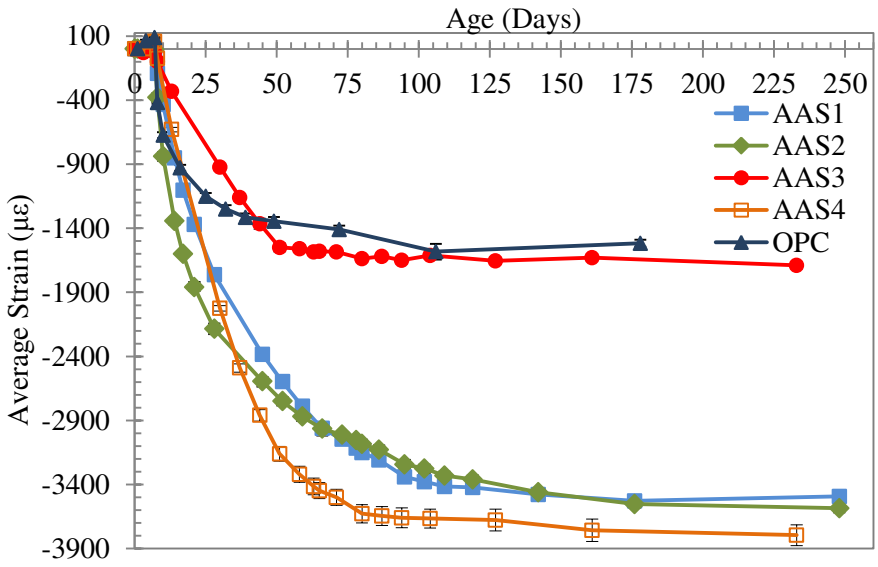

Figure 3-5. Drying shrinkage strains of AAS and OPC mortars as a function of age

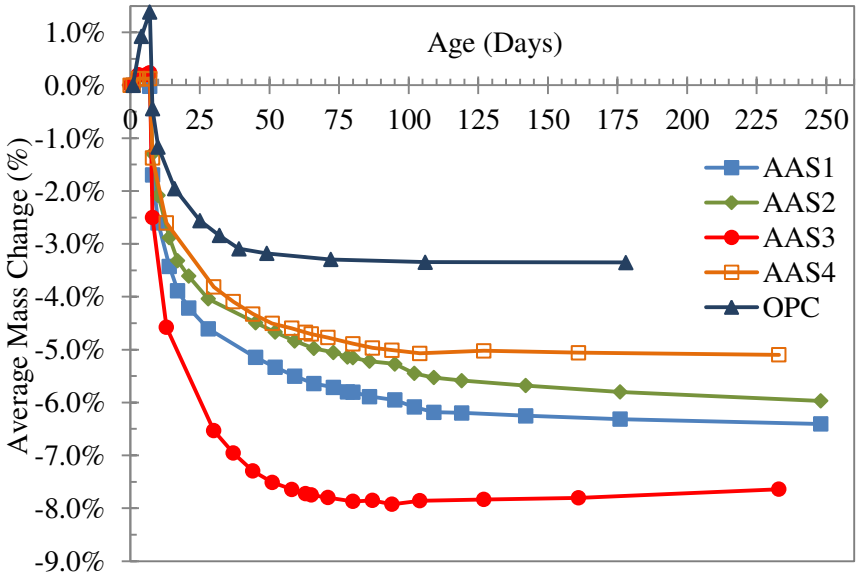

Figure 3-6. Mass change (%) with respect to day 1 (time of demolding) of AAS and OPC mortars as a function of age at 23C, 50%RH

The drying mass loss of all mixtures has been shown in Figure 3-6. For all the mass loss measurements, the coefficient of variation was less than 2.25%. As such, the error bars are not included. Every AAS mixture lost more mass than the control OPC. The OPC mortar ultimately

lost 4.7% of its 7 day (end of moist curing) mass, while AAS mortars lost 5.2% to 7.9% of their 7 day mass. Others (Melo Neto et al., 2008) have also reported high mass losses of AAS mortars after exposure to 50% RH. AAS3 had the highest mass loss of all mixtures.

Using the moisture content and porosity measurements of mortars at 7 days (i.e., end of moist curing and beginning of drying), the degree of saturation of the five mortars can be calculated as a function of age, based on their mass measurements. These results are shown in Figure 3-7. All mortars show a slightly lower than 100% saturation at the end of moist curing period (7 days). This may be attributed to self-desiccation in mortars, which could not be completely relieved by external moist curing, potentially due to a low hydraulic permeability of the mortars. It is also observed in Figure 3-7 that the ultimate degree of saturation of the OPC and AAS4 mortars are similar at 48%. The other three AAS mortars show a lower ultimate degree of saturation of 41.5% (AAS2), 38.4% (AAS1), and 29.8% (AAS3). Interestingly, AAS3 is the mortar that showed the slowest setting, lowest compressive strength and lowest drying shrinkage among the AAS mortars. This could indicate a larger porosity and pore size, which agrees with a low degree of saturation after exposure to drying at 50%RH. The water permeable porosity and degree of saturation of the moist cured and sealed mortars at 7 days are shown in Table 3-6. The sealed mortars were those cast inside corrugated tubes for autogenous shrinkage measurement. It is observed that the total porosity of mortars is generally larger for AAS mixtures in comparison with the OPC. AAS3 shows the largest porosity, which is in agreement with its slow setting and low compressive strength. All mortars that were moist cured show approximately similar degree of saturation of 92.4% to 95.8% at the end of moist curing period (7 days). However, in the case of sealed mortars, the degree of saturation of the OPC mortar is considerably lower than the AAS mixtures. This indicates a higher degree of self-desiccation in OPC, which could be the result of lower evaporable water content and a potentially higher chemical shrinkage. It should be noted that all mortars had the same volume of liquid phase and the same porosity of 27.9% at the time

of mixing (equivalent to a paste porosity of 56.5%). However, hydration of the OPC mortar may chemically bind a larger proportion of the mix water, which results in a lower porosity and lower evaporable water in comparison with the AAS mortars.

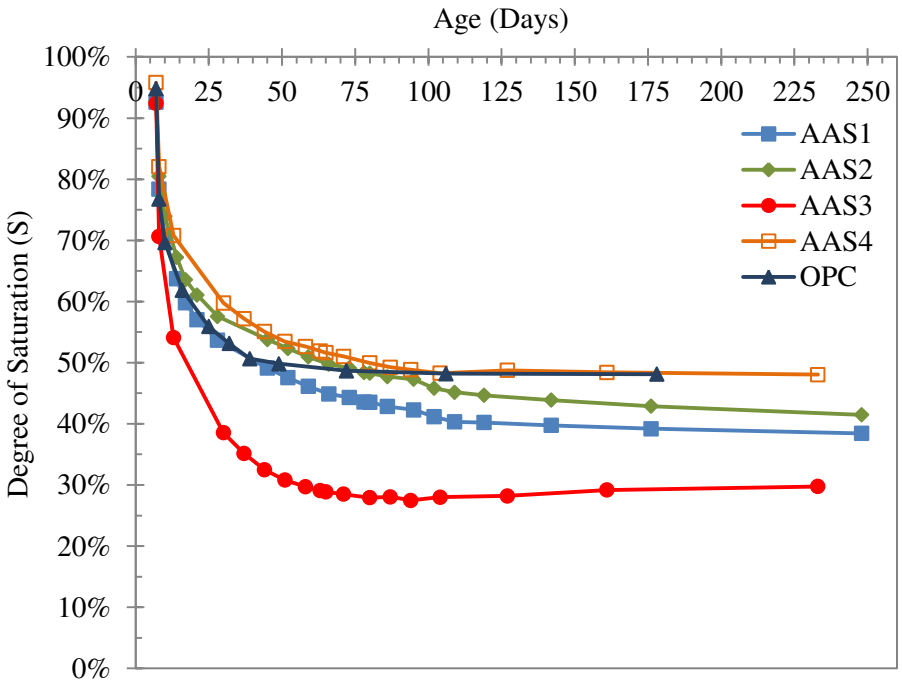

Figure 3-7. Degree of saturation (%) of AAS and OPC mortars as a function of age

Table 3-6. Degree of saturation and water permeable porosity of mortars at 7 days after casting (each data point is an average of 2 duplicate specimens)

	Mortars Moist Cured for 7 Days		Mortars Sealed for 7 Days	
Mix ID	Degree of Saturation (Vol%)	Water Permeable Porosity (Vol%)	Degree of Saturation (Vol%)	Water Permeable Porosity (Vol%)
AAS1	92.6%	25.8%	90.8%	24.8%
AAS2	92.7%	25.6%	89.3%	25.5%
AAS3	92.4%	27.4%	91.9%	27.0%
AAS4	95.8%	25.5%	97.8%	22.6%
OPC	94.8%	20.2%	75.9%	21.9%

The autogenous shrinkage of the five mortar mixtures is shown in Figure 3-8. It has been previously reported that autogenous shrinkage strains of AAS concrete can be up to 7 times larger than those found in OPC (Bakharev et al., 2000). In this work, AAS1, AAS2 and AAS4 mixtures show similarly large autogenous shrinkage of 2700 to 2800 με at 240 days. It should be noted that the drying shrinkage strains of AAS1, AA2, and AAS4 were also similarly large. AAS3 has considerably smaller but growing autogenous shrinkage strains of 826 με at 155 days. The OPC mortar has the smallest autogenous shrinkage of 415 με at 135 days.

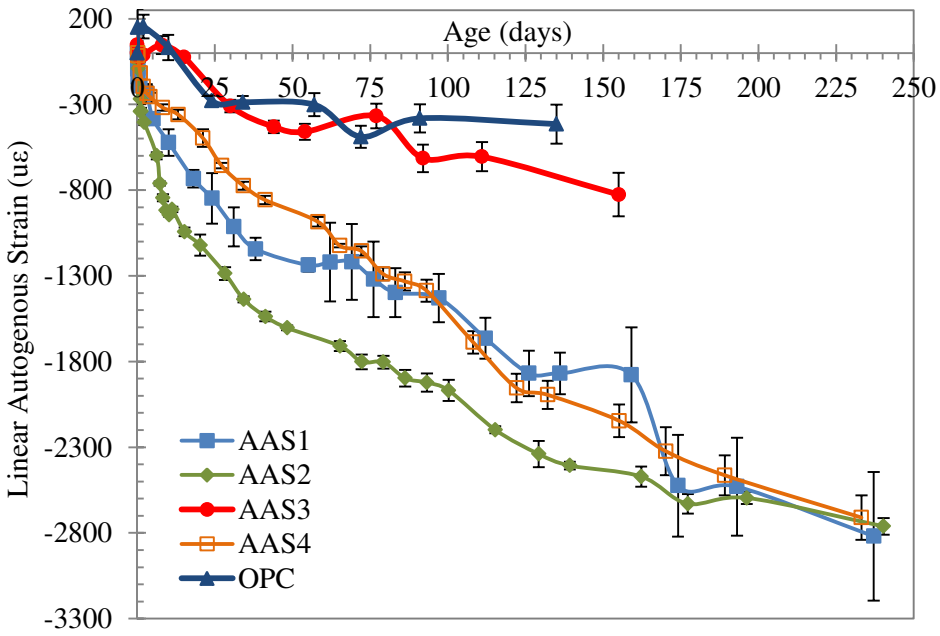

Figure 3-8. Autogenous shrinkage strains of AAS and OPC mortars

The chemical shrinkage results for the five paste specimens are reported in Figure 3-9. It can be seen that the AAS binders have practically similar chemical shrinkage of 0.031 to 0.038 ml per gram slag at 150 days. Out of these, AAS3 and AAS4 mixtures have slightly larger chemical shrinkage values, which may be due to a higher degree of slag reaction at this age. AAS4 was tested up to 14 days (336 hours); and the final measured chemical shrinkage was recorded to be 0.045 ml/g_{slag}. All AAS mixtures have lower chemical shrinkage values than the

OPC (approximately 0.057 ml/g_{cem} at 150 days). The values of chemical shrinkage at complete hydration of OPC are reported (Powers et al., 1948; Jensen et al., 2001) to be approximately 0.064 ml/g_{cem}. Similarly, the theoretical chemical shrinkage values of AAS at complete hydration have been estimated (Chen and Brouwers, 2007) to be between 0.107 and 0.139 ml/g_{slag}, depending on the concentration and type of activator used. Other authors (Thomas et al., 2012) recently calculated a similar value of 0.122 ml/g_{slag}. The measured chemical shrinkage for AAS binders does not agree with these theoretical estimations. It is possible that the measured chemical shrinkage of AAS is relatively small because at any given age, the degree of hydration of slag is considerably lower than that of OPC. The results reported in Figure 3-9 are in ml of chemical shrinkage per gram of cement or slag mixed; and does not account for the actual fraction of the cement or slag that has reacted at a given age. Ben Haha et al. (2011) have measured a 7 day degree of hydration of approximately 30% for AAS systems, much lower than that of OPC. Using the degree of hydration data from Ben Haha et al. (2011), the actual chemical shrinkage values of these AAS mixtures range from 0.103 to 0.127 ml/g_{slag}, which is close to the estimated values from Thomas et al. (2012) and Chen and Brouwers (2007). Future testing (for example using selective acid dissolution of AAS pastes to determine the exact degree of reaction of slag) is needed and will be conducted to better characterize the chemical shrinkage of AAS binders.

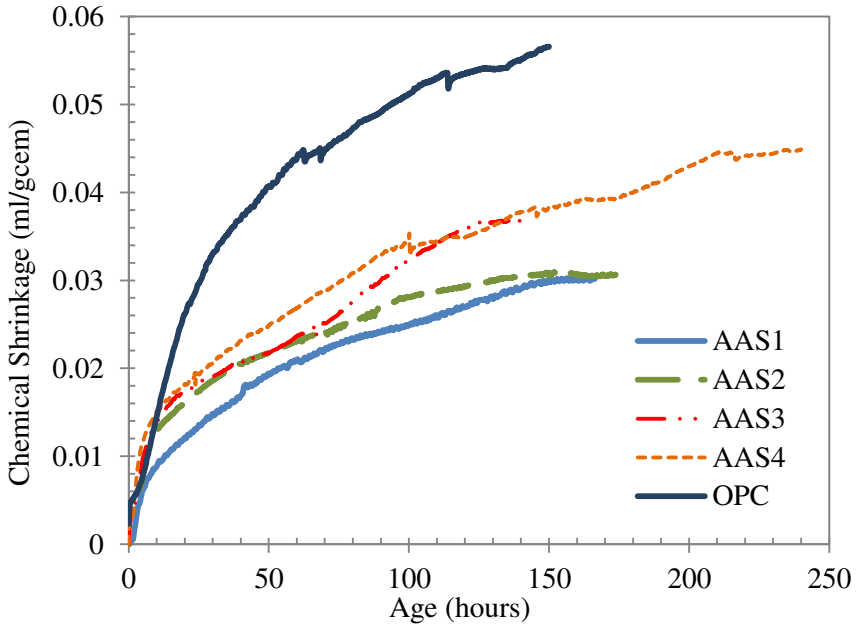

Figure 3-9. Chemical shrinkage strains of AAS and OPC pastes

3.5 Discussion

Several mechanisms have been proposed as the cause of shrinkage in cementitious materials. These include (1) capillary stress, (2) change in surface energy, (3) disjoining pressure, and (4) loss of interlayer water (Ferraris and Wittmann 1987; Mindess et al. 2003). Among these, (1) and (2) are considered to be primarily responsible for shrinkage at moderate to high relative humidities (Mindess et al. 2003). The capillary stress mechanism is due to formation of liquid-vapor menisci when pores larger than ~5nm undergo drying (Fischer and Israelachivili 1981). As such, this mechanism is responsible for shrinkage at higher RH (>~60%) (Weiss et al. 2008). In the following, the capillary stress mechanism is discussed further and linked to the observations of the drying and autogenous shrinkage in the AAS mixtures. The Mackenzie-Bentz equation (equation 3-2) (Mackenzie et al., 1950; Bentz et al., 1998) can be used to calculate the ultimate paste shrinkage due to capillary stresses (P_{cap}):

$$\varepsilon_p = \frac{S}{3} P_{cap} \left[\frac{1}{K} - \frac{1}{K_s}\right] \quad (3\text{-}2)$$

where S corresponds to the volumetric degree of saturation (as in Figure 3-7), K is the bulk elastic modulus of the paste, and K_s is the bulk modulus of the solid skeleton (e.g., C-S-H or unreacted solids). It should be noted that this equation assumes linear-elastic behaviour and does not account for creep. Nor does it account for carbonation-induced shrinkage.

For a sealed sample (i.e., the case for autogenous shrinkage), the magnitude of capillary stresses (P_{cap}), as shown by the Laplace equation (equation 3-3) (Adamson et al., 1997), is inversely proportional to the radius of the largest pore (r) emptied due to chemical shrinkage of the paste (Radlińska et al., 2008).

$$P_{cap} = -\frac{2\gamma cos\theta}{r} \quad (3\text{-}3)$$

The surface tension of the pore solution is represented as γ (typically about 0.07 N/m (Radlińska et al., 2008)), and θ is the solid-solution contact angle (assumed to be 0 radians). Capillary stresses induced by drying shrinkage are dictated by the ambient *RH* according to Kelvin's equation (equation 3-4) (Adamson et al., 1997).

$$P_{cap} = \frac{RTln\left(\frac{RH}{x_w}\right)}{V_m} \quad (3\text{-}4)$$

In Kelvin's equation, R is the universal gas constant, T (^{o}K) is the absolute temperature, V_m is the molar volume of pore solution, and x_w = (mol water/mol pore solution) accounts for the presences of ions in the pore solution, per Raoult's law (Lura, 2003). Using simple calculations, it can be shown that the value of V_m for the pore solution of mortars is close to V_m for water (18 cc/mol). Also, the molar fraction of water (x_w) in the pore solution of AAS mortars remains larger than 92.3%. As a result, it is reasonable to conclude that, according to Eq. 3-4, the magnitude of

capillary stress (P_{cap}) that is formed when AAS and OPC mortars are exposed to drying at a certain ambient relative humidity is similar in both types of mortars.

According to equations (3-2) and (3-4), a large drying shrinkage in AAS mortar could be the result of a high degree of saturation (S), or low stiffness of mortar (K). As discussed above, the capillary stress (P_{cap}) is anticipated to be similar among different mortars in the case of drying shrinkage. The results presented in Table 3-5 show that AAS3 and AAS4 mortars have approximately 33% lower stiffness, which can result in 1.5 times larger drying shrinkage according to equation 3-2, if all other parameters remain the same. A recent study (Gebregziabiher and Peethamparan, 2013) used nano-indentation to measure K_s values for AAS binders and reported these to be similar to K_s values for OPC binders. The results in Figure 3-7 suggest that AAS mortars have similar or lower degree of saturation, than the OPC mortar. However, the low saturation of AAS3 may partly explain its lower drying shrinkage comparing to other AAS mortars. Overall, the capillary stress mechanism by itself does not completely explain the cause of large drying shrinkage, especially in AAS1 and AAS2 mortars. Other mechanisms such as creep, carbonation shrinkage, and shrinkage due to change in the surface energy of the solid skeleton as it loses moisture (also known as the Gibbs-Bangham shrinkage) must be considered to fully account for the drying shrinkage behavior of AAS concrete. Specifically carbonation shrinkage may dictate the overall drying shrinkage behavior of AAS concrete. It is known that carbonation dramatically increases the drying shrinkage of concrete (Shi et al, 2006, Puertas et al, 2006), and AAS binders have carbonation rates up to 200% higher than those observed in OPC (Siddique and Khan, 2011), due to the absence of solid portlandite and a lowed C/S in C-S-H formed in AAS binders. These mechanisms are currently under investigation at Penn State.

According to equations (3-2) and (3-3), possible explanations for higher autogenous shrinkage of AAS in comparison with OPC include larger chemical shrinkage, higher degree of

saturation, a finer pore structure, and lower stiffness. The results in Figure 3-9 show a smaller chemical shrinkage measured for AAS binders. However, as discussed before, these results do not match theoretical predictions, as they don't account for the actual degree of reaction of slag. Using the degree of reaction data from Ben Haha et al. (2011), the actual chemical shrinkage values of these AAS binders range from 0.103 to 0.127 ml/g_{slag}, which matches the theoretical estimates of Thomas et al. (2012) and Chen and Brouwers (2007). If these values are trustable, the chemical shrinkage of AAS binders is considerably larger than that of OPC (0.064 ml/g_{cem}). In addition, and according to Tables 3-5 and 3-6, sealed AAS mortars have a larger degree of saturation and similar or smaller elastic stiffness, in comparison with the OPC mortar.

It has been shown (Collins and Sanjayan, 2000) that AAS pastes have a very different pore size distribution compared to OPC. OPC pastes have a large percentage of micropores (<1.25nm) and macropores (25-5000 nm), whereas AAS pastes (especially those activated by waterglass) have a large percentage of mesopores (1.25-25nm). It was reported (Ben Haha et al. 2011), that waterglass activated binders have a denser microstructure and finer porosity than AAS activated by NaOH. This is likely due to the slower dissolution of slag, and presence of dissolved silica in the pore space (contributed by the waterglass activator), which permits uniform precipitation of C-S-H and C-A-S-H within the open pore space. Conversely, NaOH activated binders often have high pH and result in rapid initial dissolution of slag and formation of hydration products on the slag surface, which act as a diffusion barrier and slows down further dissolution of slag particles (Ben Haha et al. 2011). This can create a coarser and higher porosity matrix, which in the case of AAS3, agrees with a lower compressive strength and elastic modulus, and a higher total porosity as reported in Figure 3-4 and Tables 3-5 and 3-6. At the same time, a coarser porosity could be beneficial in reducing the capillary stress (P_{cap}) that develops in a sealed system, according to equation 3-3.

Overall, a higher degree of saturation, a finer pore structure, a lower stiffness, and a potentially larger chemical shrinkage all are favourable towards a higher autogenous shrinkage in AAS mortars, and may explain the cause of large shrinkage observed in Figure 3-8. In addition, other mechanisms such as creep and the Gibbs-Bangham shrinkage may further contribute to a large autogenous shrinkage of AAS and must be considered in future research.

3.6 Conclusions

Based on the research findings in this paper, the following conclusions can be drawn:

- Depending on the activator composition, AAS mortars can exhibit lower, comparable, or higher compressive strengths than the OPC mortar of same initial porosity. High pH and high SiO_2 concentration in the activator resulted in the highest AAS strength.
- AAS mortars activated using only NaOH showed 33% lower elastic modulus than the OPC mortar, which had a similar elastic modulus as the AAS mortars activated by waterglass.
- After 7 days of moist curing AAS mortars had a larger total water permeable porosity and larger evaporable water content than the OPC, despite a similar initial porosity at the time of casting.
- The degree of saturation at 7 days was comparable among all moist cured mortars. However, when the mortars were sealed for the first 7 days, the OPC mortar showed a considerably lower saturation, indicating a higher degree of self-desiccation.
- Except AAS3, AAS mortars showed approximately two times larger drying shrinkage than the control OPC mortar. A lower elastic stiffness contributes to this large drying shrinkage; however, other mechanisms (such as carbonation) are also very likely to contribute to the high shrinkage. A coarser pore structure and lower degree of saturation

resulted in low strength and lower drying shrinkage for AAS3, which had shrinkage comparable to OPC mortar.

- Similarly, with exception of AAS3, AAS mortars exhibited considerably higher autogenous shrinkage than the control OPC mortar. A higher degree of saturation, a finer pore structure, a lower elastic stiffness, and a potentially larger chemical shrinkage all are favorable towards a higher autogenous shrinkage in AAS mortars.
- The measured chemical shrinkage of AAS paste was smaller than that of the equivalent OPC. However, this does not account for the actual mass of slag reacted at a given age. Using a 30% degree of reaction of slag at 7 days, based on the work of Ben Haha et al. (2011), the normalized chemical shrinkage of the AAS pastes is obtained as 0.103 to 0.127 ml/g_{slag}, which agrees with theoretical estimations from the literature and is much larger than the chemical shrinkage of OPC.

3.7 Acknowledgements

The authors gratefully acknowledge the financial support from the National Science Foundation (NSF) under Award CMMI #1265789. Any opinions, findings and conclusions or recommendations expressed in this material are those of the authors and do not necessarily reflect the views of the National Science Foundation. The authors are also appreciative of the invaluable assistance of Mr. Jared Wright and Mr. Dan Fura. All tests were performed at the Civil Infrastructure Testing and Evaluation Laboratory (CITEL) and the Materials Research Institute (MRI) of Penn State.

3.8 References

Adamson, A.W., Gast, A.P. (1997) Physical Chemistry of Surfaces, 6th Ed., Wiley Interscience, New York.

Ashby, M. (2009), Materials and the Environment, Elsevier, Burlington, MA.

Bakharev, T., Sanjayan, J.G., Cheng, Y.B. (2000), Effect of admixtures on properties of alkali-activated slag concrete, Cement and Concrete Research, 30, 1367-1374.

Ben Haha, M., Le Saout, G., Winnefeld, F., Lothenbach, B. (2011) Influence of activator type on hydration kinetics, hydrate assemblage and microstructural development of alkali activated blast furnace-slags, Cement and Concrete Research, 41, 301-310.

Bentz, D.P., Garboczi, E.J., Quenard, D.A. (1998) Modeling drying shrinkage in reconstructed porous materials: Application to porous Vycor glass, Modeling and Simulation in Materials Science and Engineering, 6, 211-236.

Brough, A.R., Atkinson, A. (2002)Sodium silicate-based, alkali-activated slag mortars Part I. Strength, hydration, and microstructure, Cement and Concrete Research, 32, 865-879.

Chang, J.J. (2003), A study on the setting characteristics of sodium silicate-activated slag pastes, Cement and Concrete Research, 22, 1005-1011.

Chen, W., Brouwers, H.J.H. (2007) The hydration of slag, part 1: reaction models for alkali-activated slag, Journal of Materials Science, 42, 428-443.

Cincotto, M.A, Melo A. A., Repette, W.L. (2003) Effect of different activators type and dosages and relation to autogenous shrinkage of activated blast furnace slag cement, In: G. Grieve, G. Owens, Eds, Proc. 11th International Congress on the Chemistry of Cement, Durban, South Africa, pp. 1878-1888.

Collins, F.G., Sanjayan, J.G. (1999) Workability and mechanical properties of alkali activated slag concrete, Cement and Concrete Research, 29, 455-458.

Collins, F., Sanjayan, J.G. (2000) Effect of pore size distribution on drying shrinkage of alkali-activated slag concrete, Cement and Concrete Research, 30, 1401-1406.

Damtoft, J.S., Lukasik, J., Herfort, D., Sorrentino, D., Gartner, E.M. (2008) Sustainable development and climate change initiatives, Cement and Concrete Research, 38, 115-12.

Douglas, E., Bilodeau, A., Malhotra, V.M. (1992) Properties and durability of alkali-activated slag concrete, ACI Materials Journal, 89, 509-516.

Ferraris, C.F., Wittmann, F.W. (1987) Shrinkage mechanisms of hardened cement paste, Cement and Concrete Research, 17, 453-464.

Fischer, L., Israelachivili, J. (1981) Experimental studies on the applicability of the Kelvin equation to highly curved concave menisci, Journal of Colloid and Interface Science, 80, 528-541.

Gebregziabiher, B.S., Peethamparan, S. (2013) Characterization of alkali-activated slag gel using nano-indentation, In: 3rd International Conference on Sustainable Construction Materials and Technologies (SCMT3), Kyoto, Japan.

Jennings, H.M. (1986) Aqueous solubility relationships for two types of calcium silicate hydrate, Journal of the American Ceramic Society, 69, 614-418.

Jensen, O.M., Hansen, P.F. (2001) Water-entrained cement-based materials: Principles and theoretical background, Cement and Concrete Research, 31, 647-654.

Jiang, M., Chen, X., Rajabipour, F., Hendrickson, C.T. (2014) Comparative life cycle assessment of conventional, glass powder, and alkali-activated slag concrete and mortar, ASCE Journal of Infrastructure Systems (accepted)

Lura, P. (2003) Autogenous deformation and internal curing of concrete, Doctoral Disseration, Delft University of Technology, Delft, the Netherlands.

Mackenzie, J.K. (1950) The elastic constants of a solid containing spherical holes, Proceedings of the Physical Society, 683, 2-11.

Melo Neto, A.A, Cincotto, M.A., Repette, W. (2008) Drying and autogenous shrinkage of pastes and mortars with activated slag cement, Cement and Concrete Research, 38(4) 565-574.

Mindess, S., Young, J.F., Darwin, D. (2003) Concrete, 2nd Ed., Prentice Hall, Upper Saddle River, New Jersey.

Palacios, M., Puertas, F. (2007) Effect of shrinkage-reducing admixtures on the properties of alkali-activated slag mortars and pastes, Cement and Concrete Research, 37, 691–702.

Powers, T.C., Brownyard, T.L. (1948) Studies of the physical properties of hardened Portland cement paste, Bulletin 22, Research Laboratories of the Portland Cement Association, Chicago.

Puertas, F., Palacios, M., Vazquez, T. (2006) Carbonation process of alkali-activated slag mortars, Journal of Materials Science, 41, 3071-3082.

Radlinska, A., Rajabipour, F., Bucher, B., Henkensiefken, R., Sant, G., Weiss, J. (2008) Shrinkage mitigation strategies in cementitious systems: a closer look at differences in sealed and unsealed behavior, Transportation Research Record, No. 2070, 59-67.

Ravikumar, D., Neithalath, N. (2012) Effects of activator characteristics on the reaction product formation in slag binders activated using alkali silicate powder and NaOH, Cement and Concrete Composites, 34, 809-818

Sant, G., Lura, P., Weiss, J. (2006) Measurement of volume change in cementitious materials at early ages, Transportation Research Record, No. 1979, 21-29.

Shi, C., Krivenko, P., Roy, D. (2006) Alkali-Activated Cements and Concrete, Taylor & Francis.

Siddique, R., Iqbal Khan, M. (2011)Supplementary Cementing Materials. Chapter 3: Ground Granulated Blast Furnace Slag., Springer-Verlag, Berlin Heidelberg.

Taylor, H.F.W. (1997) Cement Chemistry, 2nd Ed., Thomas Telford, London.

Thomas, J.J., Allen, A.J., Jennings, H.M. (2012) Density and water content of nanoscale solid C-S-H formed in alkali-activated slag (AAS) paste and implications for chemical shrinkage, Cement and Concrete Research, 42, 377-383.

Weiss, J., Lura, P., Rajabipour, F., Sant, G. (2008) Performance of shrinkage reducing admixtures at different humidities at early ages, ACI Materials Journal, 105, 478-486.

Chapter 4

Drying shrinkage of alkali-activated slag cements

Part 1. Characterization of drying shrinkage under various relative humidities

Christopher Cartwright[1]*, Hailong Ye[1], Farshad Rajabipour[2], Aleksandra Radlińska[3]

Keywords: Ground-granulated blast-furnace slag; Alkali-activated cement; Shrinkage; Relative Humidity; Carbonation

4.1 Abstract

This paper series contains two parts: (1) characterization of drying shrinkage of alkali-activated slag (AAS) mortars under various relative humidities and (2) understanding the mechanisms of drying shrinkage of AAS. Part one presents the unprecedented drying shrinkage results of AAS under a broad range of relative humidities. The drying shrinkage of four AAS mortars, activated by a combination of sodium hydroxide and sodium silicate, are presented and compared to a control ordinary Portland cement (OPC) mortar. A non-standardized mold was designed to cast "mini-bar" (1.27 x 1.27 x 12.7cm) mortar prisms in order to reach equilibrium quicker and avoid moisture gradients. All mixtures were dried under nitrogen purge at relative humidities of 85%, 70%, 50%, and 30%. After a constant strain had been reached at 85% RH for all mixtures, they were moved to the 70% RH chamber. This process was repeated for 50% and 30% RH to evaluate the implications of a slower drying rate. In order to quantify the effect of carbonation on drying shrinkage, a separate set of mixtures was cast and dried under air purge at

50% RH. It was found at each relative humidity that AAS mixtures lose more mass and have larger drying shrinkage deformations than OPC mixtures, regardless of the drying rate. However, the ultimate drying shrinkage values of AAS are dependent on the drying rate as these materials shrink more when the relative humidity is decreased gradually instead of rapidly. The carbonation of AAS materials increases their drying shrinkage deformations. At high relative humidities (70% RH), creep plays a significant role in the drying shrinkage of AAS. A lower elastic stiffness of mixtures activated solely by NaOH leads to a larger drying shrinkage. Other mechanisms, which are completely dissected in part two, also contribute to the high drying shrinkage measured for AAS.

4.2 Introduction

Multiple environmentally friendly products have been researched up to date to partially or fully replace the energy intensive portland cement in concrete. Research has shown [1, 2] that industrial waste products, e.g. blast furnace slag from steel manufacturing, can be used to successfully produce a portland cement-free concrete when activated by an alkaline solution (i.e., sodium hydroxide or sodium silicate). Ground granulated blast furnace slag (GGBFS) is an amorphous material mainly comprised of calcium and alumino-silicates [1]. Alkali activation is the process of exposing these glassy materials to a high pH environment to accelerate the congruent dissolution of alumino-silicates. The dissolved products can then react with water and the available alkali and calcium ions to form calcium silicate hydrate (C-S-H) and calcium-alumino-silicate hydrate (C-A-S-H) products [2]. The process of alkali activation allows for the development of an environmentally friendly portland cement-free binder.

Alkali-activated slag (AAS) concrete is a product that can offer superior properties over ordinary portland cement (OPC) concrete, including potential for high compressive strength (up

to 130 MPa) and excellent performance against fire and chemical (acid, sulfate) attack [1]. A recent environmental life-cycle assessment (LCA) study shows that AAS concrete has 73% lower greenhouse gas (GHG) emissions, 43% less embodied energy, 25% less water use, and 22 to 94% lower values of different environmental toxicity impact parameters, in comparison with OPC concretes of similar compressive strength [3]. Despite their favorable performance, the marketability and acceptance of alkali-activated concretes in the industry have been hindered partly by concerns related to their long-term durability. Perhaps one of the most significant conundrums impeding the implementation of AAS concrete is their volumetric instability.

Many researchers have reported significantly higher drying shrinkage strains in AAS compared to OPC [1, 2, 4-10]. For instance, Cartwright et al. reported the drying shrinkage strains of AAS mortars to be up to twice as large as the corresponding OPC mortar when dried under a relative humidity of 50%. Palacios and Puertas also reported significantly higher drying shrinkage strains for AAS mortar compared to OPC mortar. While limited data of the drying shrinkage performance of AAS materials do exist [1, 2, 4-10], the scientific reasoning and mechanisms of the large strains have not been explained. For example, many authors hypothesize that upon drying, a high capillary force forms in the materials fine pore structure and is the main driving force for the drying shrinkage of AAS concrete [5, 10]. However, the current lack of research data and understanding of the shrinkage performance of AAS concrete over a broad range of relative humidities (i.e., between 30% and 100%) limits the validity of this hypothesis. The aforementioned knowledge gap needs to be bridged before AAS concrete can become a marketable and viable alternative to the energy intensive OPC concrete.

The compressive strength, time of setting, and autogenous, drying, and chemical shrinkage of four AAS and one OPC mortar mixtures have previously been measured and documented [4]. This manuscript presents the advanced drying shrinkage characterization of those mixtures. It

develops the relationships between drying shrinkage, mass loss, rate of drying, and relative humidity. Conclusions are then drawn based on the observed experimental results. Subsequently, the second part of this paper series measures the pore structure of each mixture via mercury intrusion porosimetry (MIP), characterizes theoretical drying shrinkage mechanisms of AAS materials (using MIP data), and compares these calculations to the results of this research.

4.3 Experimental

4.3.1 Materials

Alkali-activated slag mortar mixtures were investigated in this study. The grade 120 (ASTM C989M-12a) ground granulated blast-furnace slag had a density of 2.89 g/cm^3 and an oxide composition as shown in Table 4-1. A particle size analysis (using laser diffraction) showed that 50% of slag particles were smaller than 7.4μm and 10% of slag particles were smaller than 1μm. The portland cement used in this study was an ASTM C150 type I cement with a density of 3.14 g/cm^3 and an oxide composition as shown in Table 4-1. A quantitative analysis on XRD of slag powder was performed and found a mainly amorphous material with trace amounts of crystalline calcium sulfate ($CaSO_4$) and tri-calcium silicate (Ca_3SiO_5).

Table 4-1. Oxide compositions of slag and portland cement (mass %)

	CaO	SiO_2	Al_2O_3	MgO	SO_3	Fe_2O_3	Na_2O	K_2O	LOI
Slag (GGBFS)	47.5	30.8	11.45	3.65	3.03	1.81	0.17	0.38	1.17
Type I cement	62.5	19.9	5.44	2.31	4.93	2.26	0.30	0.89	0.86

Four AAS mortars and a control OPC mortar were designed using a constant volumetric liquid (water + activator) to solid (slag or cement) ratio of 1.30, yielding an initial binder porosity of 56.5%. For the control OPC mixture, this is equivalent to a mass-based w/c = 0.414. For the

AAS mixtures, the mass-based liquid to solid ratio was in the range 0.489 to 0.510, depending on the concentration and density of the activating solutions (Tables 4-2 and 4-3). The aforementioned liquid to binder ratios are paste properties; therefore, they are independent of any aggregate absorption. For all mixtures, a natural river sand meeting ASTM C33M-11a requirements was used. The sand had a fineness modulus 2.60, oven dry specific gravity 2.52, and absorption capacity 2.02%. Each mortar mixture was designed with a 50.7% volume fraction of sand. The mixture proportions of the mortars are listed in Table 4-2.

Table 4-2. Mortar mixture proportions (per liter of mortar)

<table>
<tr><th>Mix ID</th><th>NaOH (g)</th><th>$Na_2O(SiO_2)_n$ (g)</th><th>Water* (g)</th><th>Cement (g)</th><th>Slag (g)</th><th>Sand (g)</th></tr>
<tr><td>Control (OPC mortar)</td><td>0</td><td>0</td><td>296.8</td><td>656.6</td><td>0</td><td rowspan="5">1,247</td></tr>
<tr><td>AAS1</td><td>23.77</td><td>35.70</td><td>263.6</td><td rowspan="4">0</td><td rowspan="4">603.9</td></tr>
<tr><td>AAS2</td><td>5.94</td><td>95.49</td><td>234.6</td></tr>
<tr><td>AAS3</td><td>23.77</td><td rowspan="2">0</td><td>285.9</td></tr>
<tr><td>AAS4</td><td>47.54</td><td>274.8</td></tr>
</table>

*Note: Water content includes absorption by oven dry sand

Table 4-3. Activating solution properties for AAS mixtures

Mix ID	$n = (SiO_2/Na_2O)$ molar-based	pH	Density (g/cc)	WRA (mL/kg_{slag})
AAS1	0.41	14.31	1.09	5.00
AAS2	1.22	13.78	1.13	2.00
AAS3	0	14.30	1.04	4.15
AAS4	0	14.60	1.09	8.00

Mortars AAS1 (lower silica concentration) and AAS2 (higher silica concentration) were activated using an alkaline solution which contained a combination of dissolved sodium hydroxide (NaOH) pellets, aqueous sodium silicate ($Na_2O(SiO_2)_n$) (waterglass), and water. Mortars AAS3 and AAS4 were activated using only a solution of NaOH in water (either 2M or 4M). The aqueous sodium silicate (($Na_2O(SiO_2)_n$) had the modulus n = 1.60, pH = 13.7, and specific gravity = 1.60 at 20°C. It contained 53.2% water, 28.8% SiO_2, and 18.0% Na_2O by mass.

4.3.2 Test Procedures

4.3.2.1. Mixing

To prepare the activating solutions, reagent sodium hydroxide pellets were first dissolved in water at room temperature while sealed to prevent carbonation, which would decrease the solutions pH. The solution was shaken for 5 minutes and then set aside for approximately two hours to cool. For mortars AAS1 and AAS2, the sodium hydroxide and sodium silicate solutions were kept separate. The correct dosage of WRA was added to the activating solution (NaOH portion) before mixing. Once all ingredients were ready for mixing, the activating solution, slag, and sand were poured into an electric (Hobart) mixer and mixed at slow speed (140 ± 5 rev/min) and medium speed (285 ± 5 rev/min) according to ASTM C305-12. In order to allow the sodium hydroxide solution to properly dissolve the slag, the sodium silicate was excluded from the mixture until 15 minutes after mixing. The sand was oven dry but cooled in advance to room temperature. The mortar proportions reported in Table 4-2 account for the absorption of water (or the activating solution) by the sand.

4.3.2.2. Flow tests

Each mortar mixture was tested and adjusted to a flow of 100% (ASTM C1437-07) to ensure comparable workability. The AAS mixtures had lower workability than the corresponding OPC mixture; therefore, a small dosage of high range water reducing admixture was added when needed. Individual WRA dosages per mixture can be found in Table 4-3. For mortars AAS1 and AAS2, the entire WRA dosage was added to the sodium hydroxide solution before adding the sodium silicate solution.

4.3.2.3. Drying shrinkage tests

A non-standardized mold was designed to cast "mini-bar" prism samples (1.27 × 1.27 × 12.7 cm). Mini-bars (Figure 4-1) were used in order to reach equilibrium quicker and avoid moisture gradients. The chambers were capable of creating environments under various humidities and/or gases (e.g., nitrogen and air purge). The PVC mold was able to be completely disassembled and had a gage length of four inches. The gage studs used were one inch black oxide alloy #6-32 set screws. Length measurements were taken utilizing a modified digital comparator with an invar (low coefficient of thermal expansion) place holder and a measuring accuracy of 0.0001 inch.

Figure 4-1. "Mini-bar" cast for drying shrinkage

Environmental chambers were programmed for four different humidities (85%, 70%, 50%, and 30%) and constant temperature (23±0.5°C). The drying shrinkage (rapid drying) was measured for all five mixtures (four samples per mixture) at each humidity under dry nitrogen (N_2) purge after seven days of moist curing (100% RH, 23±0.5°C). The concentration of CO_2 in environmental chambers was recorded with a portable CO_2 analyzer as 0ppm. The specimen dried at 85% RH were measured until a constant length was reached, at which point the humidity was dropped to 70% RH. This step-wise drying procedure was repeated for 50% and 30% RH as well. A separate set of mixtures was tested at 50% RH in air (P_{CO2} recorded as 400ppm) to observe the effect of carbonation on drying shrinkage and mass loss. Simultaneous mass measurements were taken using a high precision balance with an accuracy of 0.01g to determine the moisture loss upon drying.

4.3.2.4. Elastic modulus

Elastic modulus was measured for all five mortar mixtures according to ASTM C469. The test was performed using two duplicate 100×200 mm cylinders per mixture. The mortar cylinders

were demolded at 24 hours and moist cured until moments before testing at 28-days. Each cylinder was placed in a dual compressometer-extensometer, connected to a data acquisition system. This setup logged the longitudinal displacement readings through the use of LVDTs while the specimen was loaded in compression at a load rate of 0.25±0.05 MPa/sec. This measurement takes into effect the elastic region from the point of 50 micro-strains to 40% of the ultimate (failure) load for the age tested, otherwise known as the chord modulus.

4.3.2.5. Moisture content

The moisture content of each mortar mixture was measured according to ASTM C642-13. After 7 days of moist curing, all samples were oven dried at 105°C until constant mass was achieved. The mortar was then submerged in water for 48 hours after which the samples were surface dried and mass was recorded. The samples were then placed in water and boiled for 5 hours; afterwards, they were surface dried and the mass was recorded. Finally, the samples were suspended by a wire in a water bath and their buoyant mass was measured.

4.4 Results

4.4.1 Drying shrinkage in nitrogen

4.4.1.1. Rapid drying

Figure 4-2 shows the results of the measured (rapid) drying shrinkage for all mortar mixtures. Except for AAS3 at 30% RH, AAS mixtures show higher drying shrinkage strains than the control OPC mix at all humidities. OPC shows increasing shrinkage strains with a decreasing

relative humidity (the largest shrinkage deformations are observed at the lowest humidity), which is consistent with the findings of other authors [11-12]. However, the AAS mixtures show different drying behavior than that of OPC. Although all mixtures were dried under a relative humidity of 30%, the largest ultimate drying shrinkage strain of mixtures AAS3 (1850με) and AAS4 (1950με) is observed at 70% RH; similarly, AAS1 (2100με) and AAS2 (2275με) shrink the most at 50% RH. This unique shrinkage behavior (the largest shrinkage deformations are not observed at the lowest humidity) of AAS mortars differs significantly from that of OPC.

Figure 4-3 presents the mass loss data of the four AAS and the control OPC mixtures. Each AAS mixture lost more mass under a given relative humidity than OPC. This contradicts the findings of Collins and Sanjayan who measured lower mass loss upon drying for AAS than OPC. At every relative humidity, AAS3 showed the largest mass loss of all mixtures. This is likely due to the coarse porosity of the paste in AAS3.

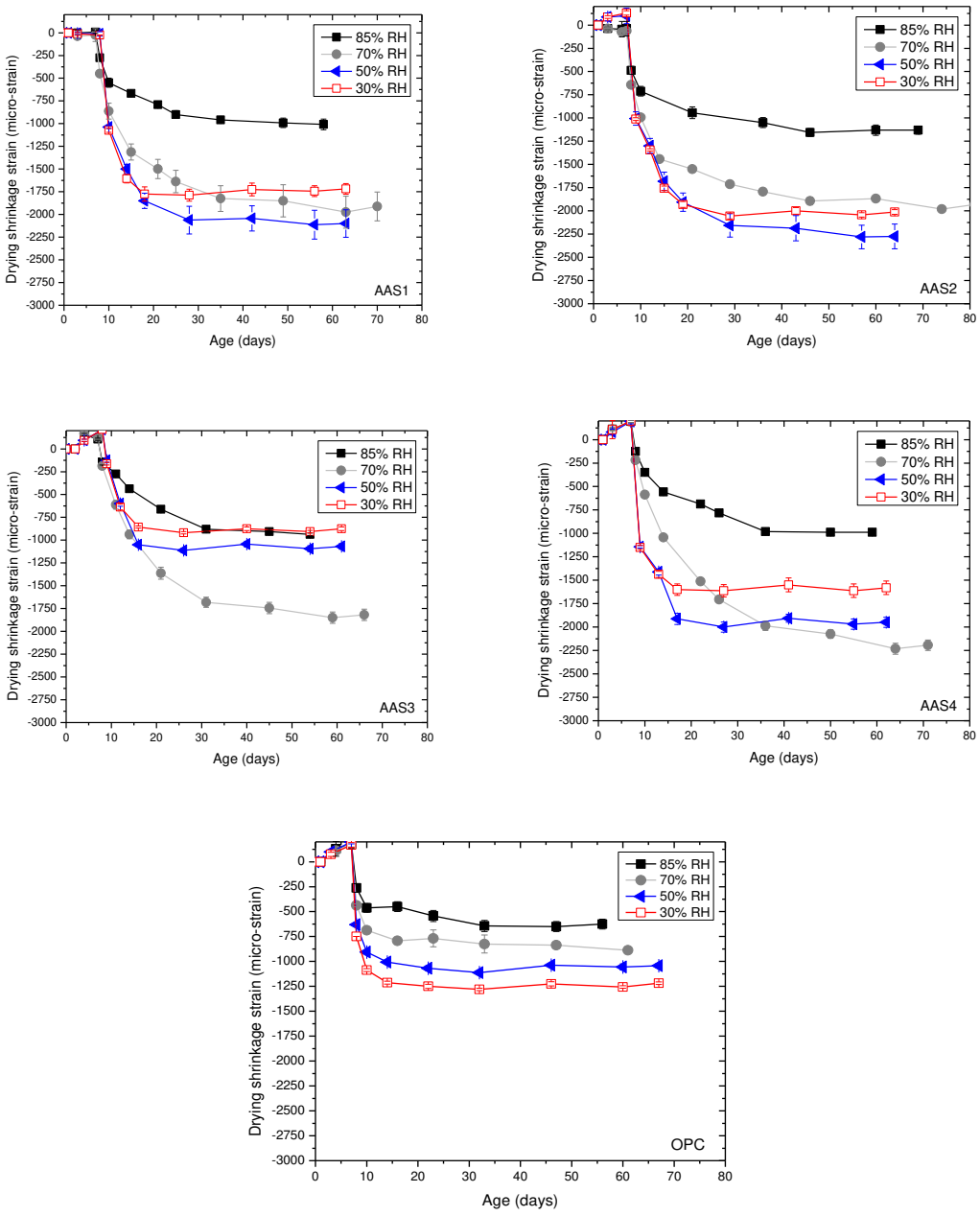

Figure 4-2. Drying shrinkage strains under nitrogen purge for all mortar mixtures

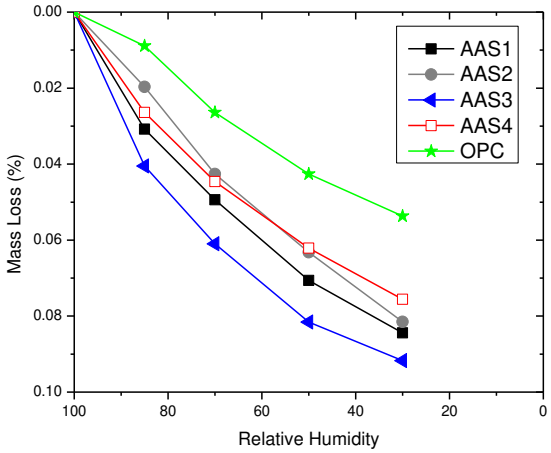

Figure 4-3. Mass loss (%) vs. relative humidity for all mortar mixtures

4.4.1.2. Step-wise drying

Figure 4-4 displays the results of the step-wise drying procedure used to evaluate all five mortar mixtures. Similar to rapid drying, the control OPC showed lower drying shrinkage strains and mass loss than all AAS mixtures at every humidity. The AAS mortars activated solely by NaOH (AAS3 and AAS4) show the highest drying shrinkage of all AAS mixtures, though the difference between the four is marginal.

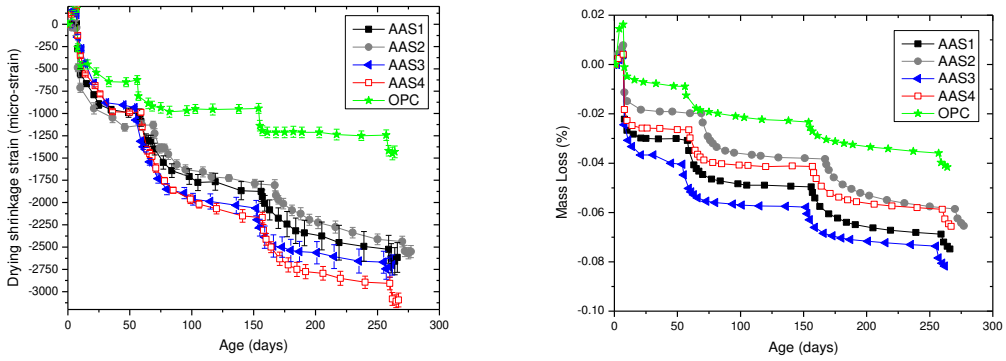

Figure 4-4. Drying shrinkage and mass loss of mortar mixtures using the step-wise procedure.

When dried gradually under the step-wise process, the relationship between shrinkage and relative humidity for AAS materials differs significantly from rapid drying. For example, when dried rapidly to a relative humidity of 50%, AAS3 shows an ultimate shrinkage of 1500 με; however, when dried gradually to 50% RH, the same mixture shows 77% higher shrinkage deformations (2650 με). Similar tendencies are observed for the other AAS mixtures. All mixtures lost slightly less mass during the step-wise drying compared to the direct drying process. Clearly, the drying shrinkage behavior of AAS materials is highly dependent on the rate of drying.

4.4.2. Drying shrinkage in air

Figure 4-5 shows the results of drying shrinkage and mass loss of all five mixtures dried at 50% RH under air purge and nitrogen purge. Each of the five mixtures shows larger drying shrinkage deformations and slightly less mass loss when dried in an environment containing CO_2, both of which are consistent with the findings of other scientists [11]. When dried in ambient conditions (P_{CO2} = 400 ppm; 50% RH), AAS1 showed drying shrinkage strains of 3700με, 1600με higher than the same mixture dried in nitrogen (P_{CO2} = 0 ppm; 50% RH). Similarly, the shrinkage deformations of AAS4 increased by 1183με while AAS2 and AAS3 each saw increases of approximately 825με. OPC showed the smallest increase of approximately 550 με (51.7% higher) when dried in air, which is consistent with previously reported data [12].

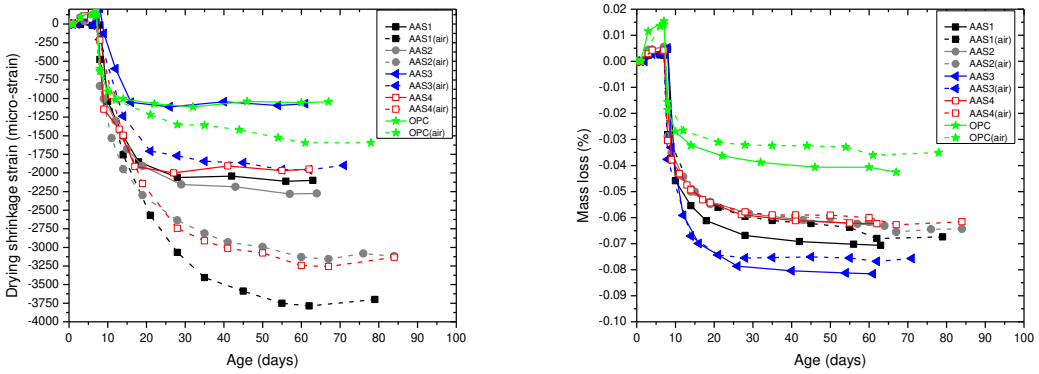

Figure 4-5. Drying shrinkage and mass loss of mortar mixtures dried under air and nitrogen.

4.4.3. Elastic modulus

The values for 28-day static elastic modulus of all five mixtures are presented in Table 4-4. The results show that AAS3 and AAS4 have a smaller elastic modulus (approximately 13.5 GPa) than the other three mixtures (ranging from 19.49 to 20.71 GPa). AAS1, AAS2, and OPC show similar elastic modulus values at 28 days. Assuming a similar Poisson's ratio for all mortars, it can be inferred that the bulk modulus of mortars AAS3 and AAS4 is approximately 67% of that of the other three mortars.

Table 4-4. Modulus of elasticity of mortars at 28 days

Mix ID	Modulus of Elasticity (GPa)
AAS1	20.71
AAS2	19.85
AAS3	13.25
AAS4	13.55
OPC	19.49

4.4.4. Degree of saturation

Using the moisture content measurements of mortars at 7 days (i.e., end of moist curing and beginning of drying), the degree of saturation of the five mortars can be calculated based on their mass measurements. These results are shown in Table 4-5. All mortars show a slightly lower than 100% saturation at the end of the moist curing period (7 days). This may be attributed to self-desiccation in mortars, which could not be completely relieved by external moist curing, potentially due to a low hydraulic permeability of the mortars. Table 4-5 shows that OPC has the highest degree of saturation among all 5 mixtures at every relative humidity. It is also observed that AAS3 shows the lowest degree of saturation at every humidity. Interestingly, AAS3 is the mortar that showed the slowest setting, lowest compressive strength, and lowest drying shrinkage among the AAS mortars [4]. This could indicate a larger porosity and pore size, which agrees with a low degree of saturation after exposure to drying. The other three AAS mortars show degree of saturation values between OPC and AAS3. It should be noted that all mortars had the same volume of liquid phase and the same porosity of 27.9% at the time of mixing (equivalent to a paste porosity of 56.5%).

Table 4-5. Ultimate degree of saturation (Vol %) of mortars

Mix ID	100% RH (Moist Cure)	85% RH	70% RH	50% RH	30% RH
AAS1	92.6%	63.4%	47.5%	29.1%	17.5%
AAS2	92.7%	69.9%	51.6%	35.5%	19.3%
AAS3	92.4%	57.2%	40.1%	23.5%	15.1%
AAS4	95.8%	67.9%	52.6%	35.3%	22.5%
OPC	94.8%	70.1%	52.1%	37.8%	27.6%

4.5 Discussion

4.5.1. Mass loss, drying shrinkage, and relative humidity

The correlation between relative humidity and drying shrinkage for all five mortar mixtures can be viewed in Figure 4-6. For the direct drying process, the OPC mixture shows a bi-linear relationship between relative humidity and drying shrinkage, which was similarly measured and reported by other authors [11]. However, AAS mixtures show a parabolic relationship between ultimate shrinkage and relative humidity. The direct drying process resulted in a decrease in shrinkage deformations of AAS after a certain relative humidity had been reached. For example, AAS1 and AAS2 showed highest shrinkage at 70% RH, and AAS3 and AAS4 showed highest shrinkage at 50% RH, even though all five mixtures were dried to 30% RH. This behavior suggests that different shrinkage mechanisms operate at various relative humidities. It is likely that the forces resulting from the capillary stress mechanism govern AAS shrinkage behavior at high humidities. However, this mechanism fails to create these high stresses at lower humidities due to the breakdown of the menisci in the capillaries. As a result, shrinkage behavior of AAS in lower humidity environments is probably dictated by other shrinkage mechanisms (such as Gibbs-Bangham) that produce relatively smaller shrinkage stresses than the capillary stress mechanism.

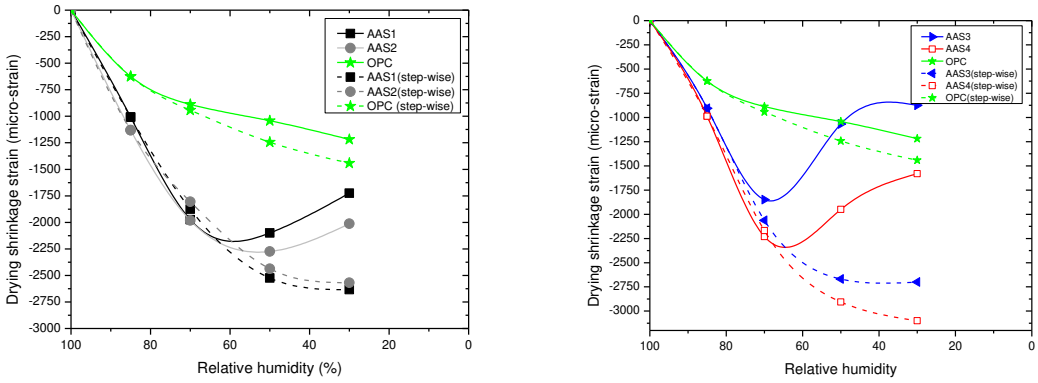

Figure 4-6. Drying shrinkage vs relative humidity for all mortar mixtures

Interestingly, when dried under the step-wise process, the shrinkage behavior of AAS was found to differ significantly compared to rapid drying (i.e., the highest drying shrinkage deformations were observed at the lowest relative humidity). This may be due to the formation of irreversible shrinkage strains during the gradual drying process. At the relative humidities where the highest shrinkage stresses exist (i.e., 70% and 50% for AAS as concluded in Fig. 4-2 and Fig. 4-6), it is possible that a rearrangement of the C-S-H and C-A-S-H particles occurs due to additional bond formations between particles upon closer particle contact during drying [11, 13]. Because the samples were slowly dried under high stress environments (70% and 50% RH), the step-wise process may have induced particle rearrangement and irreversible shrinkage strains that were not formed during the rapid drying process. This explains why shrinkage deformations in AAS mixtures do not decrease (as observed in rapid drying) when slowly dried to a lower relative humidity.

When dried slowly during the step-wise procedure, each mixture lost slightly less mass compared to those dried rapidly. This is likely due to either increased hydration during the slower drying process or microcracking during the rapid drying process. Because mixtures were held at higher humidities for a longer period of time during the step-wise process, the C-S-H and C-A-S-

H gels may have been able to incorporate a larger quantity of non-evaporable water into the hydration products. This would result in a smaller amount of mass loss compared to the direct drying process. Additionally, micro-cracking may play a role in the larger mass loss observed during the rapid drying process. The rapid drying creates stress gradients over the width of the mini-bars. Since AAS materials show a high risk of cracking [1], it is likely that micro-cracks form in the paste and facilitate the diffusion of evaporable moisture through the system [11].

4.5.2. Carbonation shrinkage

Carbonation of cementitious materials occurs when atmospheric $CO_{2(g)}$ dissolves in pore solution and forms carbonic acid, which then attacks calcium bearing phases present in the cementitious paste (i.e., CH, C-S-H, and C-A-S-H) [14, 15]. Also known as decalcification, this process lowers the C/S ratio of the paste and forms a soft silica gel prone to high drying shrinkage strains.

As reported in section 3.2, AAS mortars can shrink up to 1600με more when dried in ambient conditions compared to a CO_2 free environment. Many scientists [14, 16] have reported that alkali-activated slag cements experience intense carbonation rates (up to 200% higher than Portland cement). As suggested by Shi et al., high carbonation in AAS is probably due to the limited formation of solid CH and the low calcium to silica ratio ($C/S_{AAS} \approx 0.96$ to 1.3 [17]) of its paste; C/S_{OPC} is generally higher than 1.5 [1,18-19]. Decalcification of C-S-H only occurs when solid CH is inaccessible or locally depleted [18]; therefore, the limited amount of CH in AAS cements does not mitigate carbonation of C-S-H gel as it does in OPC. This likely explains the high carbonation shrinkage observed in this study; however, further research, which is currently under investigation at Penn State, is needed to fully understand the carbonation of AAS materials and its effect on drying shrinkage.

4.5.3. Creep, stiffness, and effective stress

4.5.3.1. Creep

Creep, the gradual increase in deformation under a constant stress, plays a significant role in the drying shrinkage of AAS. Figure 4-7 displays the drying shrinkage of mortar mixtures as a function of their degree of saturation. All AAS mortars show significant shrinkage strains up to and after the point of equilibrium for the degree of saturation. This is strong evidence that these mixtures are experiencing additional deformations due to creep. The OPC mortar shows very little additional shrinkage deformations after the degree of saturation has reached equilibrium. AAS mixtures (especially AAS3 and AAS4) appear to show the highest amount of creep at higher humidities (i.e., 85% RH and 70% RH) and seem to stop shrinking after a certain degree of saturation, approximately 40%, has been reached. It is likely that one (or multiple) shrinkage mechanism ceases to exist below this degree of saturation threshold. Theoretical calculations testing this theory will be performed in part two.

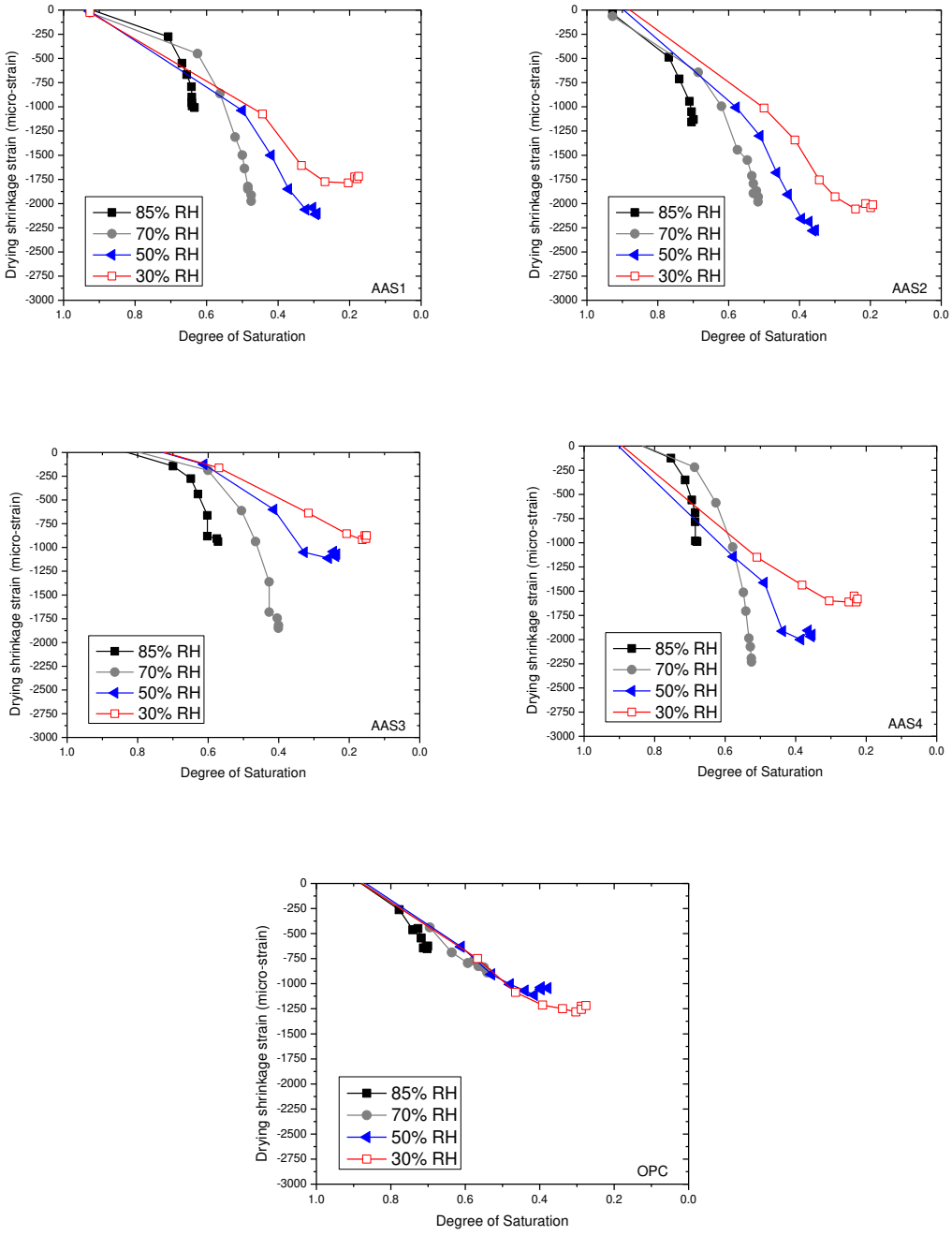

Figure 4-7. Shrinkage vs. degree of saturation for all mortar mixtures

4.5.3.2. Stiffness

The Mackenzie-Bentz equation [20-21] (equation 4-1) can be used to calculate the ultimate paste shrinkage due to capillary stresses (P_{cap}) induced by drying:

$$\varepsilon_p = \frac{S}{3} P_{cap} \left[\frac{1}{K} - \frac{1}{K_s}\right] \quad (4\text{-}1)$$

where S corresponds to the volumetric degree of saturation (as in Table 4-5), K is the bulk elastic modulus of the paste (as in Table 4-4), and K_s is the bulk modulus of the solid skeleton (e.g., C-S-H or unreacted solids). It should be noted that this equation assumes linear-elastic behavior and does not account for creep or carbonation-induced shrinkage. P_{cap} is anticipated to be similar among all mortars investigated in this research [4].

According to equation (4-1), a large drying shrinkage in AAS mortar could be the result of a high degree of saturation (S) or low stiffness of mortar (K). The results in Table 4-5 show that AAS mortars have a similar or lower degree of saturation than the OPC mortar at every relative humidity, which would eliminate the degree of saturation as a primary cause of large shrinkage in AAS. However, the low saturation of AAS3 may partly explain its lower drying shrinkage comparing to other AAS mortars. A recent study [22] used nano-indentation to measure K_s values for AAS binders and reported these to be similar to K_s values for OPC binders.

The results presented in Table 4-4 show that AAS3 and AAS4 mortars have approximately 33% lower stiffness (K), which results in 1.5 times larger drying shrinkage according to equation 4-1, if all other parameters remain the same. However, as discussed in section 3.3, the stiffness values of AAS1 and AAS2 are similar to that of OPC; therefore, they are not responsible for the large shrinkage observed in mixtures activated by sodium hydroxide and sodium silicate.

4.5.3.3. Effective stress

The effective stress in equation 4-1 can be calculated by combining the degree of saturation (S) (Table 4-5) with the capillary pressure (P_{cap}). P_{cap} can be estimated for mortars that are drying using the ambient relative humidity (RH) and Kelvin's equation [23] (equation 4-2):

$$P_{cap} = \left[\frac{RTln(RH)}{V_w}\right] \quad (4\text{-}2)$$

where V_w is the molar volume of the pore fluid (assumed equal to the molar volume of water, 18.02 x 10^{-6} m^3/mol); R is the ideal gas constant, 8.314 J/(mol·K); and T (K, R) is the absolute temperature. The resulting effective stress ($S \cdot P_{cap}$) is plotted against the ambient relative humidity (RH) in Fig. 4-8 for all five mortars. It should be noted that AAS1 has an identical plot to AAS4 and thus is hidden behind AAS4 in Fig. 4-8. It can be seen that the capillary stress effect seems to plateau for AAS mixtures as the RH approaches 30% RH. However, the effective stress for the control OPC mortar continues to increase as the RH is dropped to 30% RH. This indicates that the low degree of saturation (S) (Table 4-5) of AAS mortars limits the potential maximum stress induced by the capillary stress mechanism at low relative humidities (i.e. 30% and 50% RH). This plateau of effective stress at 30% RH for AAS mixtures validates the unique shrinkage behavior observed in Fig. 4-6.

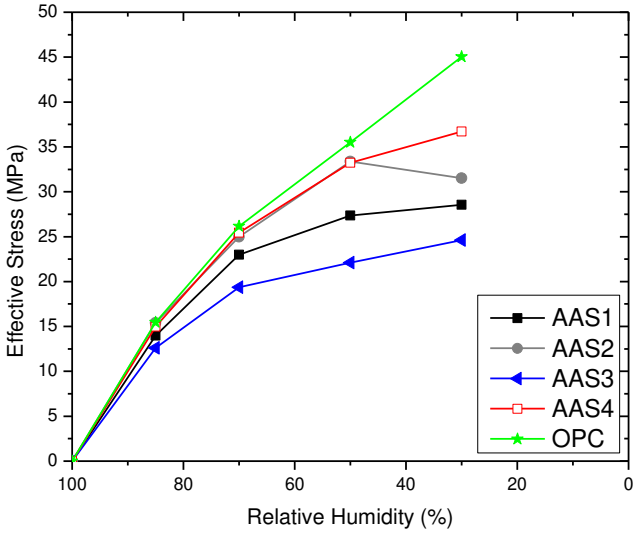

Figure 4-8. Effective stress vs. relative humidity for all mortar mixtures.

4.6 Conclusions

- Except for AAS3 at 30% RH, AAS mixtures have higher drying shrinkage strains than the control OPC at 85%, 70%, 50%, and 30% RH.
- AAS mixtures have a unique parabolic relationship between relative humidity and ultimate drying shrinkage that differs significantly from the bi-linear correlation of the OPC mixture.
- The drying shrinkage of AAS is highly dependent on the rate of drying (i.e., larger drying shrinkage strains are observed at a given RH when the material is dried slowly), which may be a result of the development of irreversible shrinkage.
- When dried under ambient conditions (P_{CO2} = 400 ppm; 50% RH), AAS mortars showed up to 75% larger drying shrinkage deformations than drying under nitrogen purge (P_{CO2} = 0 ppm; 50% RH). This suggests that carbonation of AAS materials drastically

increased the drying shrinkage; however, further research is needed to fully understand the mechanisms of carbonation shrinkage.

- AAS mixtures (especially at 70% RH) show increasing shrinkage strains at a constant degree of saturation. Increasing deformations under a given stress implies that creep plays a significant role in the drying shrinkage process of AAS materials, especially at high relative humidities.
- Compared to the OPC mortar, all AAS mixtures showed a relatively lower degree of saturation during drying.
- AAS mortars activated using only NaOH showed 33% lower elastic modulus than the OPC mortar, which had a similar elastic modulus as the AAS mortars activated by waterglass. The lower elastic modulus of AAS3 and AAS4 contributes to the higher shrinkage deformations of these mixtures; however, it cannot explain the high shrinkage of AAS1 and AAS2.

4.7 Acknowledgements

The authors gratefully acknowledge the financial support from the National Science Foundation (NSF) under Award CMMI #1265789. Any opinions, findings and conclusions or recommendations expressed in this material are those of the authors and do not necessarily reflect the views of the National Science Foundation. The authors are also appreciative of the invaluable assistance of Mr. Jared Wright and Mr. Dan Fura. All tests were performed at the Civil Infrastructure Testing and Evaluation Laboratory (CITEL) and the Materials Research Institute (MRI) of Penn State.

4.8 References

[1] Shi, C., Krivenko, P., Roy, D. (2006) Alkali-Activated Cements and Concrete, Taylor & Francis.

[2] Ben Haha, M., Le Saout, G., Winnefeld, F., Lothenbach, B. (2011), Influence of activator type on hydration kinetics, hydrate assemblage and microstructural development of alkali activated blast furnace-slags. Cement and Concrete Research, 41, 301-310.

[3] Jiang, M., Chen, X., Rajabipour, F., Hendrickson, C.T. (2014) Comparative life cycle assessment of conventional, glass powder, and alkali-activated slag concrete and mortar, ASCE Journal of Infrastructure Systems (accepted).

[4] Cartwright, C., Rajabipour, F., Radlińska, A. (2014) Shrinkage characteristics of alkali-activated slag cements, ASCE Journal of Materials in Civil Engineering (accepted).

[5] Melo Neto, A.A, Cincotto, M.A., Repette, W. (2008) Drying and autogenous shrinkage of pastes and mortars with activated slag cement, Cement and Concrete Research, 38(4) 565-574.

[6] Douglas, E., Bilodeau, A., Malhotra, V.M. (1992) Properties and durability of alkali-activated slag concrete, ACI Materials Journal, 89, 509-516.

[7] Bakharev, T., Sanjayan, J.G., Cheng, Y.B. (2000), Effect of admixtures on properties of alkali-activated slag concrete, Cement and Concrete Research, 30, 1367-1374.

[8] Palacios, M., Puertas, F. (2007) Effect of shrinkage-reducing admixtures on the properties of alkali-activated slag mortars and pastes, Cement and Concrete Research, 37, 691–702.

[9] Cincotto, M.A, Melo A. A., Repette, W.L. (2003) Effect of different activators type and dosages and relation to autogenous shrinkage of activated blast furnace slag cement, In: G. Grieve, G. Owens, Eds, Proc. 11th International Congress on the Chemistry of Cement, Durban, South Africa, pp. 1878-1888.

[10] Collins, F., Sanjayan, J.G. (2000) Effect of pore size distribution on drying shrinkage of alkali-activated slag concrete, Cement and Concrete Research, 30, 1401-1406.

[11] Mindess, S., Young, J.F., Darwin, D. (2003) Concrete, 2nd Ed., Prentice Hall, Upper Saddle River, New Jersey.

[12] Verbeck, G.J. (1958) Carbonation of hydrated Portland cement, ASTM Sp. Tech. Publ. No. 205, pp. 17-36.

[13] Neville, A.M. (2006), Properties of Concrete 4th Ed., Pearson Education Limited, London, England.

[14] Siddique, R., Iqbal Khan, M. (2011)Supplementary Cementing Materials. Chapter 3: Ground Granulated Blast Furnace Slag., Springer-Verlag, Berlin Heidelberg.

[15] Bakharev, T., Sanjayan, J.G., Chen, Y.B. (2001) Resistance of alkali-activated slag concrete to carbonation, Cement and Concrete Research, 31, 1277-1283

[16] Puertas, F., Palacios, M., Vazquez, T. (2006) Carbonation process of alkali-activated slag mortars, Journal of Materials Science, 41, 3071-3082.

[17] Chen, W., Brouwers, H.J.H. (2007) The hydration of slag, part 1: reaction models for alkali-activated slag, Journal of Materials Science, 42, 428-443.

[18] Taylor, H.F.W. (1997) Cement Chemistry, 2nd Ed., Thomas Telford, London.

[19] Jennings, H.M. (1986) Aqueous solubility relationships for two types of calcium silicate hydrate, Journal of the American Ceramic Society, 69, 614-418.

[20] Mackenzie, J.K. (1950) The elastic constants of a solid containing spherical holes, Proceedings of the Physical Society, 683, 2-11.

[21] Bentz, D.P., Garboczi, E.J., Quenard, D.A. (1998) Modeling drying shrinkage in reconstructed porous materials: Application to porous Vycor glass, Modeling and Simulation in Materials Science and Engineering, 6, 211-236.

[22] Gebregziabiher, B.S., Peethamparan, S. (2013) Characterization of alkali-activated slag gel using nano-indentation, In: 3rd International Conference on Sustainable Construction Materials and Technologies (SCMT3), Kyoto, Japan.

[23] Adamson, A.W., Gast, A.P. (1997) Physical Chemistry of Surfaces, 6th Ed., Wiley Interscience, New York.

Chapter 5

Measuring the chemical shrinkage of alkali-activated slag cements using the buoyancy method

Christopher Cartwright, Farshad Rajabipour, and Aleksandra Radlińska

Manuscript accepted by the Ninth International Conference on Creep, Shrinkage, and Durability Mechanics (CONCREEP-9); September 22-25, 2013; Cambridge, MA

5.1 Abstract

Recent incentives to reduce the carbon footprint of Portland cement (PC) concrete have sparked the research and development of eco-friendly products such as alkali-activated slag (AAS) concrete. AAS is a promising product capable of developing compressive strengths comparable to PC concrete; however, its large drying and autogenous shrinkage (the latter being the focus of this paper) have impeded its marketability and use in the construction industry. The mechanisms and parameters that control the self-desiccation of AAS are relatively unknown. Chemical shrinkage, the driving force of autogenous shrinkage, has never been measured for AAS systems; however, it has been theoretically estimated to be much higher than that of PC. The first step in determining why the autogenous shrinkage of AAS is so large is to investigate its chemical shrinkage. This research focuses on proper measurement of the chemical shrinkage of AAS and the parameters that affect the results.

5.2 Introduction

Concrete production utilizes the most abundant natural materials present on the Earth's surface. However, the high temperatures (~1400°C) required during production of Portland cement in the kiln result in a significant energy use (embodied energy = 5.7MJ/kg of cement) and a large CO_2 footprint (0.95kg CO_2/kg of cement) (Ashby 2009, Marinshaw and Wallace 1994). Recent global initiatives to reduce the carbon footprint and harmful emissions into the Earth's environment have ignited the research to develop new environmentally friendly and sustainable construction materials. The annual production of concrete exceeds 10^{10} tonnes/year, more than all other manmade materials combined (Ashby 2009). This large production rate results in a large carbon footprint of Portland cement, resulting in approximately 5% of the total anthropogenic GHG emissions (Damtoft et al. 2008).

Multiple eco-friendly products have been researched up to date to partially or fully replace Portland cement in concrete. Research has shown (Ben Haha et al. 2011, Shi et al. 2006) that industrial waste products, e.g. blast furnace slag from steel manufacturing, can be used to successfully produce a Portland cement-free concrete.

Alkali activation is the process of exposing a glassy silica-based material (e.g., slag) to a high pH environment to promote the congruent dissolution of alumino-silicates. These dissolved products can then react with water and the available alkali and calcium ions to form calcium silicate hydrate (C-S-H) and calcium-aluminum-silicate hydrate (C-A-S-H) gels that provide the binder phase in concrete (Ben Haha et al. 2011). The process of alkali activation of these amorphous materials allows for the development of a Portland cement-free binder (Shi et al. 2006).

The marketability and acceptance of alkali-activated slag (AAS) in the industry have been hindered by concerns related to their volumetric instability and risk of cracking. Many

researchers (Shi et al. 2006, Palacios et al. 2007, Collins et al. 2000, Chen et al. 2007) have shown that AAS concrete has significantly higher shrinkage strains (both autogenous and drying) than ordinary Portland cement (OPC) mixtures. This large deformation can lead to concrete durability issues, as cracking is expected to occur when volumetric changes are restrained. These cracks allow salts and other harmful chemicals to penetrate the concrete and corrode the reinforcing steel.

Figure 5-1 shows the autogenous shrinkage strains of several AAS and a control OPC mixture (all having a sand volume fraction of 50.7%). It can be seen that the autogenous shrinkage strains of AAS are significantly higher than those found in OPC. While limited data related to shrinkage performance of AAS do exist (Shi et al. 2006, Palacios et al. 2007), the scientific reasoning and mechanisms of large autogenous strains in AAS have not been explained. For instance, many authors (Melo Neto et al. 2008, Collins et al. 2000, Palacios et al. 2007) suggest that a refined pore structure creates large capillary stresses, resulting in a significant shrinkage of AAS systems. Others (Thomas et al. 2012) have theoretically estimated the chemical shrinkage values of AAS paste to be between 0.107 and 0.139 ml/g_{slag} and suggested that a large chemical shrinkage (in comparison with that of Portland cement: ~0.064 ml/g_{cem}) could be responsible for large autogenous shrinkage. However, a comprehensive study that physically measures the chemical shrinkage of AAS, and investigates the parameters affecting the results, has not been performed. In order to properly analyze and understand the autogenous shrinkage of AAS systems, the first step is to properly quantify and evaluate their chemical shrinkage.

This paper focuses primarily on chemical shrinkage and the role it plays in the self-desiccation of AAS systems. It provides the results for chemical shrinkage and other tests used to analyze and understand the hydration of several AAS mixtures. Chemical shrinkage and degree of

hydration experiments were conducted on four unique AAS mixtures, and the results were compared to those of a typical OPC mix.

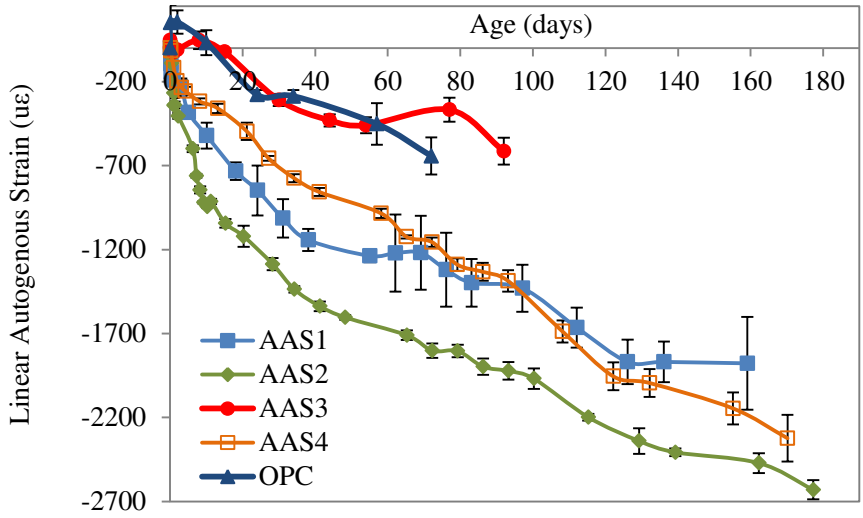

Figure 5-1. Autogenous shrinkage strains of AAS mortars

5.3 Materials

Alkali-activated slag pastes were investigated in this study. The grade 120 ground granulated blast-furnace slag used (ASTM C989M-12a) had a density of 2.89 g/cm^3, and an oxide composition as shown in Table 5-1. A particle size analysis (using laser diffraction) showed that 50% of slag particles were smaller than 7.4μm and 10% of slag particles were smaller than 1μm. Portland cement was ASTM C150 type I cement with a density of 3.14 g/cm^3 and an oxide composition as shown in Table 5-1.

Table 5-1. Oxide compositions of slag and cement (mass%)

	CaO	SiO_2	Al_2O_3	MgO	SO_3	Fe_2O_3
Slag	39.20	33.22	20.56	2.86	4.16	0
Type I cement	62.50	19.90	5.44	2.31	4.93	2.26

Four AAS mixtures and a control OPC mixture were designed using a constant volumetric liquid (water + activator) to solid (slag or cement) ratio of 1.30, yielding an initial binder porosity of 56.5%. For the control OPC mixture, this is equivalent to a mass-based w/c = 0.414. For the AAS mixtures, the mass-based liquid to solid ratio was in the range 0.489-0.510, depending on the concentration and density of the alkali activating solutions (Table 5-2).

Mixtures AAS1 (low silica concentration) and AAS2 (high silica concentration) were activated using an alkaline solution containing a combination of dissolved sodium hydroxide (NaOH) pellets, aqueous sodium silicate ($Na_2O(SiO_2)_n$), and water. The other two mixes, AAS3 and AAS4, were activated using only a solution of NaOH in water (either a 2M or 4M). The aqueous sodium silicate (($Na_2O(SiO_2)_n$) had the modulus n = 1.6, pH = 13.7, and specific gravity = 1.60 at 20°C. It contained 53.2% water, 28.8% SiO_2, and 18.0% Na_2O by mass. To prepare the activating solutions, reagent NaOH pellets were dissolved in water at room temperature and covered to prevent carbonation. The solution was shaken for 5 minutes and then set aside for approximately two hours to allow for heat dissipation and a return to room temperature. For mixtures AAS1 and AAS2, the sodium hydroxide and sodium silicate solutions were kept separate. The sodium hydroxide solution and slag were added to the mixing bowl and mixed according to ASTM C305-12. In order to allow the solution to properly dissolve the slag, the sodium silicate was excluded from the mixture until 15 minutes after mixing.

Table 5-2. Activating solution properties for AAS mixtures

Mix ID	n = (SiO_2/Na_2O) molar-based	pH	Density (g/cc)
AAS1	0.41	14.31	1.09
AAS2	1.22	13.78	1.13
AAS3	0	14.30	1.04
AAS4	0	14.60	1.09

5.4 Experimental Methods

Chemical shrinkage was measured using the buoyancy method (Sant et al. 2005). After mixing slag with the activating solution, a slag paste sample (both 10 and 25 gram samples were tested) was placed in a crystallizing dish (70 mm diameter × 50 mm height). A 10 mL solution composed of NaOH and water, with the equivalent pH of the activating solution, was placed on top of the sample. The dish was then filled with low density paraffin oil (0.863 g/cm^3). The sample was placed on a wire mesh and lowered into a stainless steel bucket filled with the oil. The bucket was placed in a water bath which was kept at constant temperature of 23±0.5°C. The wire mesh was attached to a string mounted to the underside of a high precision balance, capable of measuring mass with an accuracy of 0.0001g. The entire system was surrounded by a clear acrylic shield to prevent wind currents from interfering with the mass measurements. Mass measurements were recorded every five minutes using an automatic data acquisition system. Chemical shrinkage strains were calculated using equation 5-1 (Sant et al. 2005) where $W_{sub}(30)$ is the submerged weight of the sample 30 minutes after mixing, $W_{sub}(t)$ is the submerged weight of the sample at any time t, ρ_{oil} is the density of the paraffin oil, and g_{slag} is the mass of slag in the paste sample.

$$V_{cs} = \frac{\Delta V_{paste}}{g_{slag}} = \frac{W_{sub}(t) - W_{sub}(30)}{\rho_{oil} * g_{slag}} \tag{5-1}$$

Degree of hydration was measured using selective acid dissolution (Luke and Glasser 1987). Hydration products of AAS systems dissolve in acid; therefore, any remaining residue after acid dissolution tests represents unhydrated slag. After the chemical shrinkage test had concluded, the paste sample was removed from the setup and oven dried to constant mass. Next, the sample was crushed to a powder, and a 0.5g sample was added to a solution of EDTA, Na_2CO_3, triethanolamine, and distilled water (as prepared by Luke and Glasser, 1987). Before

adding the powder, the solution was adjusted to a pH of 11.6 using 1M NaOH. The solution was shaken for 30 minutes and then filtered through a Gooch crucible with GF/F (0.7μm diameter) filter paper and dried to constant mass.

5.5 Results & Discussion

Chemical shrinkage results for 25g (5mm thick) samples are reported in Figure 5-2. The values reported are in ml of chemical shrinkage per gram of cement or slag mixed. This does not account for the actual fraction of the cement or slag that has reacted at a given age; therefore, degree of hydration is needed to correct the chemical shrinkage for the actual amount of reacted slag or cement. It can be seen that AAS3 and AAS4 mixtures have comparable chemical shrinkage values that are lower (0.03 ml/g_{slag}) than the control OPC paste (0.055ml/g_{cem}) at 150 hours. AAS4 was tested up to 14 days (336 hours); and the final measured chemical shrinkage was recorded to be 0.045 ml/g_{slag}. Mixtures activated only by NaOH have slightly higher chemical shrinkage than those activated by NaOH and $Na_2O(SiO_2)_n$. This may be due to the coarser porosity (and therefore higher permeability) of NaOH activated systems.

The values of chemical shrinkage at complete hydration of OPC are reported (Powers et al. 1948, Jensen et al. 2001) to be approximately 0.064 ml/g_{cem}. Similarly, the theoretical chemical shrinkage of AAS at complete hydration has been estimated (Chen 2007) to be between 0.107 and 0.139 ml/g_{slag}, depending on the concentration and type of activator used. Other authors (Thomas et al. 2012) calculated a similar value of 12.2 ml/g_{slag}. Hypotheses as to why measurements of AAS chemical shrinkage in this study do not match the theoretical estimations are discussed below.

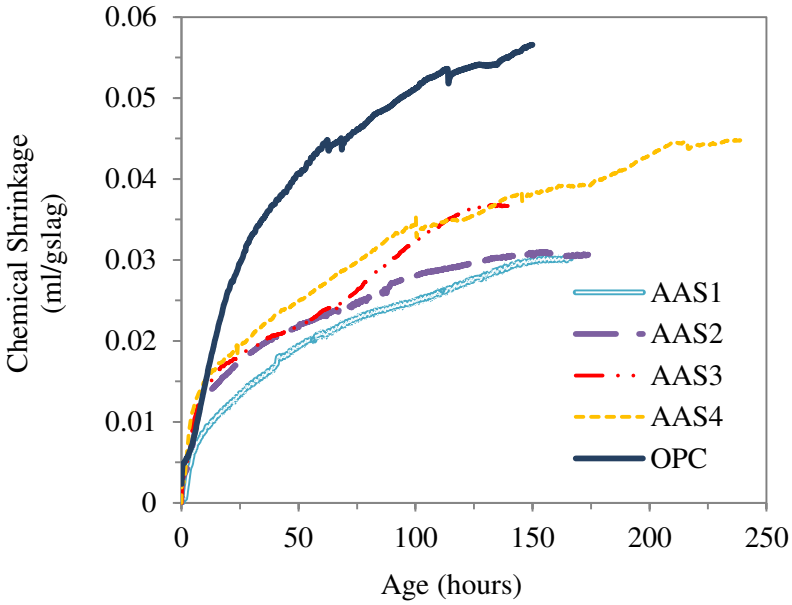

Figure 5-2. Chemical shrinkage of 25g samples

Three possible explanations for inconsistencies between the measured chemical shrinkage and the theoretical models are provided as follows: (1) only a percentage of slag particles has reacted and is available to form C-S-H and C-A-S-H products. The theoretical models assume full hydration of slag, yet previous tests (Ben Haha et al. 2011) show that AAS systems only reach approximately 40% hydration, (2) the low permeability of AAS pastes is preventing the top layer of solution in the test setup from permeating into the entire thickness of the paste and reaching all air pockets that form during slag hydration and the resulting chemical shrinkage, and (3) the large thickness (5mm) of the paste sample exacerbates the low AAS permeability and further reduces the ability of the test setup to effectively measure chemical shrinkage.

Adjustments were made to sample preparations during the chemical shrinkage test setup to test hypotheses (2) and (3). First, the sample thickness was reduced from 5mm to 2mm. This will help by eliminating the need for the top solution layer to have to permeate the entire 5 mm

thickness of the AAS paste. Second, the porosity of the mixtures was doubled to increase the paste permeability. The chemical shrinkage is reported on a "per gram of slag" basis; therefore, theoretically, the chemical shrinkage should be independent of water/solid and the porosity. An increase in the porosity, however, will increase the permeability and allow easier moisture transport from the top layer of solution into the AAS paste sample.

To evaluate hypothesis (1), tests for measuring the degree of hydration of slag were performed on each mixture after the termination of chemical shrinkage tests (typically 7 days). A low degree of hydration, as suggested by the literature, would help resolve the resounding issue as to why the chemical shrinkage values of AAS binders are significantly lower than what the theoretical models suggest.

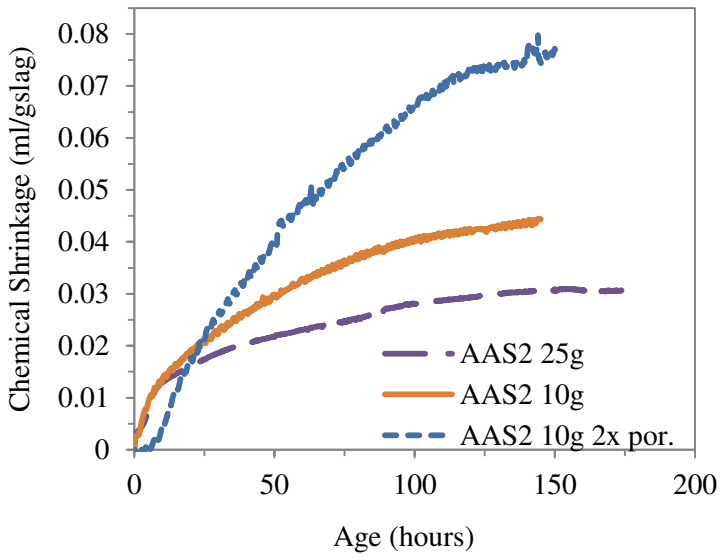

Figure 5-3. Chemical shrinkage of mix AAS2 using a thinner sample (10 grams) and a higher porosity (2x por.)

The paste AAS2 was selected for testing of a 2mm sample thickness (10 grams), an increase (2x's) in porosity, and comparison of results with those for 5 mm thick sample. The chemical shrinkage measurements for "AAS2 25g", "AAS2 10g", and "AAS2 10g 2x por" are shown in Figure 5-3. As shown previously in Figure 5-2, the 7 day chemical shrinkage of AAS2

25g is approximately 0.03 ml/g_{slag}. When the thickness of the sample was reduced to 2mm, the measured chemical shrinkage of AAS2 at 7 days increased to 0.045 ml/g_{slag}. Although this is a modest increase, the measured values are still significantly lower than the theoretical estimates. When the porosity was doubled, the chemical shrinkage for "AAS2 10g 2x por" increased to 0.08 ml/g_{slag}. This most likely occurs because the paste permeability is increased, which facilitates better moisture transport through the paste thickness. It is also possible that the hydration reactions and therefore, the degree of hydration of slag have increased due to improved accessibility of slag particles to the activating pore solution. A higher degree of hydration of slag would further increase the chemical shrinkage. These results suggest that the thickness and permeability of the AAS paste have a considerable impact on the measured value of chemical shrinkage.

Table 5-3 shows the results of selective dissolution tests to determine the degree of slag hydration for 6 AAS pastes. The tests were performed immediately after termination of the chemical shrinkage tests (typically 7 days). In addition, the raw CS results at the conclusion of the test are included, as well as the normalized results, which were adjusted based on the slag degree of hydration. Clearly, these AAS systems have a very low degree of hydration. As such, it is misleading to assume that the raw CS results from the buoyancy test can represent the true chemical shrinkage corresponding to 100% hydration of slag in alkali activated mixtures. After 7 days, half of the mixtures failed to reach 15% hydration. AAS2 10g had a slightly higher degree of hydration than AAS2 25g, most likely because a larger percentage of the thinner sample was accessible to the top layer of solution. Similarly, AAS2 10g 2x por (25.18%) had a higher degree of hydration than AAS2 10g (13.33%), due to the improved accessibility of slag particles to the activating pore solution. AAS4 had the highest degree of hydration (24.47%) among the binders with an equivalent initial capillary porosity, most likely due to its high pH and fast dissolution of slag powder.

Table 5-3. Degree of hydration of AAS pastes

	AAS1 25g	AAS2 25g	AAS2 10g	AAS2 10g 2x por	AAS3 25g	AAS4 25g
Slag Degree of Hydration	13.99%	12.03%	13.33%	25.18%	13.80%	24.47%
Raw CS (ml/g_{slag})	0.03	0.03	0.045	0.08	0.03	0.045
Normalized* CS (ml/g_{slag})	0.214	0.249	0.337	0.319	0.217	0.184

* Assumes 100% hydration of slag

The normalized chemical shrinkage values of AAS pastes are ranging from 0.184 to 0.337 ml/g_{slag} (averaged 0.253 ml/g_{slag}). These are considerably higher than the theoretical estimations, and further research is needed to determine the causes of disagreement. One reason for this discrepancy could be that absorption of free water by the aqueous sodium silicate pore solution in pastes AAS1 and AAS2 could by itself result in chemical shrinkage independent of degree of slag hydration. Another possibility could be that lower porosity AAS pastes may never reach 100% hydration due to running out of capillary pore space to form the hydration products.

5.6 Conclusions

- Chemical shrinkage (CS) of alkali activated slag (AAS) paste, when measured using the buoyancy method, is substantially lower than the values estimated based on theory. Possible reasons for such low CS measurements include: (1) low permeability of AAS paste, (2) large sample thickness, and (3) incomplete hydration of slag particles.
- Increasing the porosity of the paste sample and reducing the sample thickness both resulted in considerable increase in the chemical shrinkage results.

- At the conclusion of CS buoyancy test, only 12% to 25% of slag had reacted. Therefore, the raw chemical shrinkage results cannot represent the true CS values of slag corresponding to 100% reaction.
- After adjusting for the degree of hydration, the average chemical shrinkage of AAS paste is determined as 0.253 ml/g_{slag}. This is 3.95 times larger than the chemical shrinkage of Portland cement, and contributes directly to the large autogenous shrinkage of AAS materials.

5.7 Acknowledgements

Financial support from the National Science Foundation (NSF) under Grant No. CMMI 1265789 granted to the last two authors is greatly appreciated. Any opinions, findings and conclusions or recommendations expressed in this material are those of the authors and do not necessarily reflect the views of the NSF.

5.8 References

Ashby, M. (2009) *Materials and the Environment*, Elsevier, Inc, Burlington, MA

Ben Haha, M., Le Saout, G., Winnefeld, F., Lothenbach, B. (2011), "Influence of activator type on hydration kinetics, hydrate assemblage and microstructural development of alkali activated blast furnace-slags." Cem Conc Res, 41: 301-310.

Chen, W., Brouwers, H.J. (2007), "The hydration of slag, part 1: reaction models for alkali-activated slag." J Mater Sci, 42: 428-443.

Collins, F., Sanjayan, J.G. (2000), "Effect of pore size distribution on drying shrinkage of alkali-activated slag concrete." Cem Conc Res, 30: 1401-1406.

Damtoft, J., Lukasik, J., Herfort, D., Sorrentino, D., Gartner, E. (2008) "Sustainable development and climate change initiatives." Cem Conc Res, 38: 115-12.

Marinshaw, R., Wallace, D., (1994). "Emission factor documentation: Portland cement manufacturing." United States Environmental Protection Agency (EPA), www.epa.gov/ttn/chief/ap42/ch11/bgdocs/b11s06.pdf (accessed May 15, 2013).

Jensen, O.M., Hansen, P.F. (2001) "Water-entrained cement-based materials: Principles and theoretical background." Cem Conc Res, 31: 647-654.

Luke, K, Glasser, F.P. (1987) "Selective dissolution of hydrated blast furnace slag cements." Cem Conc Res, 17: 273-282.

Melo Neto, A.A, Cincotto, M.A., Repette, W. (2008) "Drying and autogenous shrinkage of pastes and mortars with activated slag cement." Cem Conc Res 38(4): 565-574.

Palacios, M., Puertas, F. (2007) "Effect of shrinkage-reducing admixtures on the properties of alkali-activated slag mortars and pastes." Cem Conc Res 37: 691–702.

Powers, T.C., Brownyard, T.L. (1948) "Studies of the physical properties of hardened portland cement paste." Bulletin 22, Research Laboratories of the Portland Cement Association, Chicago.

Sant, G., Lura, P., Weiss, J. (2005) "Measurement of volume change in cementitious materials at early ages." Trans Res Board. No. 1979, pp. 21-29.

Shi, C., Krivenko, P., Roy, D. (2006) *Alkali-Activated Cements and Concrete*, Taylor & Francis. New York, NY.

Thomas, J.J., Allen, A.J., Jennings, H.M. (2012) "Density and water content of nanoscale solid C-S-H formed in alkali-activated slag (AAS) paste and implications for chemical shrinkage." Cem Conc Res 42: 377-383.

Chapter 6

Conclusions and Future Research

6.1 Conclusions

This study has shown that alkali-activated slag systems have great potential for usage in the construction industry. Compressive strength and workability properties have matched or exceeded those seen in ordinary Portland cement systems; however, AAS has shown to be volumetrically unstable even in sealed conditions. Listed below are the major findings of the research presented in this thesis:

- Depending on the activator composition, AAS mortars can exhibit lower, comparable, or higher compressive strengths than the OPC mortar of same initial porosity. High pH and high SiO_2 concentration in the activator resulted in the highest AAS strength.
- AAS mortars activated using only NaOH showed 33% lower elastic modulus than the OPC mortar, which had a similar elastic modulus as the AAS mortars activated by waterglass.
- After 7 days of moist curing AAS mortars had a larger total water permeable porosity and larger evaporable water content than the OPC, despite a similar initial porosity at the time of casting.
- The degree of saturation at 7 days was comparable among all moist cured mortars. However, when the mortars were sealed for the first 7 days, the OPC mortar showed a considerably lower saturation, indicating a higher degree of self-desiccation.
- Except AAS3, AAS mortars showed approximately two times larger drying shrinkage than the control OPC mortar. A lower elastic stiffness contributes to this large drying shrinkage. A coarser pore structure and lower degree of saturation resulted in low

strength and lower drying shrinkage for AAS3, which had shrinkage comparable to OPC mortar.

- Similarly, with exception of AAS3, AAS mortars exhibited considerably higher autogenous shrinkage than the control OPC mortar. A higher degree of saturation, a finer pore structure, a lower elastic stiffness, and a potentially larger chemical shrinkage all are favourable towards a higher autogenous shrinkage in AAS mortars.
- Except for AAS3 at 30% RH, AAS mixtures have higher drying shrinkage strains than the control OPC at 85%, 70%, 50%, and 30% RH.
- AAS mixtures have a unique parabolic relationship between relative humidity and ultimate drying shrinkage that differs significantly from the bi-linear correlation of the OPC mixture.
- The drying shrinkage of AAS is highly dependent on the rate of drying (i.e., larger drying shrinkage strains are observed at a given RH when the material is dried slowly), which may be a result of the development of irreversible shrinkage.
- When dried under ambient conditions (P_{CO2} = 400 ppm; 50% RH), AAS mortars showed up to 75% larger drying shrinkage deformations than drying under nitrogen purge (P_{CO2} = 0 ppm; 50% RH). This suggests that carbonation of AAS materials drastically increased the drying shrinkage; however, further research is needed to fully understand the mechanisms of carbonation shrinkage.
- AAS mixtures (especially at 70% RH) show increasing shrinkage strains at a constant degree of saturation. Increasing deformations under a given stress implies that creep plays a significant role in the drying shrinkage process of AAS materials, especially at high relative humidities.
- Compared to the OPC mortar, all AAS mixtures showed a relatively lower degree of saturation during drying.

- AAS mortars activated using only NaOH showed 33% lower elastic modulus than the OPC mortar, which had a similar elastic modulus as the AAS mortars activated by waterglass. The lower elastic modulus of AAS3 and AAS4 contributes to the higher shrinkage deformations of these mixtures; however, it cannot explain the high shrinkage of AAS1 and AAS2.
- Chemical shrinkage (CS) of alkali activated slag (AAS) paste, when measured using the buoyancy method, is substantially lower than the values estimated based on theory. Possible reasons for such low CS measurements include: (1) low permeability of AAS paste, (2) large sample thickness, and (3) incomplete hydration of slag particles.
- Increasing the porosity of the paste sample and reducing the sample thickness both resulted in considerable increase in the chemical shrinkage results.
- At the conclusion of CS buoyancy test, only 12% to 25% of slag had reacted. Therefore, the raw chemical shrinkage results cannot represent the true CS values of slag corresponding to 100% reaction.
- After adjusting for the degree of hydration, the average chemical shrinkage of AAS paste is determined as 0.253 ml/g_{slag}. This is 3.95 times larger than the chemical shrinkage of Portland cement, and contributes directly to the large autogenous shrinkage of AAS materials.

6.2 Future Research and Potential Mitigation Strategies

This study has discovered many of the shrinkage characteristics and mechanisms of alkali-activated slag cements. Listed below is future research needed to continue the pursuit of fully understanding the shrinkage characteristics of alkali-activated slag cements.

- Characterize drying shrinkage under various relative humidities in air. Total drying shrinkage in concrete is a combination of carbonation and moisture loss. In order to separate the two mechanisms and properly determine which one contributes the most to drying shrinkage, testing in air must be performed to compare to shrinkage dried under nitrogen. This involves testing "mini-bar" samples under air purge at 85%RH, 70%RH, 50%RH, and 30%RH. The results of these tests will provide a clear indication on the contribution of total drying shrinkage from carbonation and moisture loss and can lead to the implementation of effective mitigation tools for drying shrinkage in AAS systems.

Using the results obtained from this research, certain shrinkage mitigation strategies can be suggested for investigation. The following list includes possible mitigation tools that may be used to mitigate AAS shrinkage and help create a more marketable product:

- Internal curing using lightweight aggregate (LWA) is a proven strategy in Portland cement concrete that reduces autogenous strains. LWAs contain large pores and, when pre-soaked, act as large "reservoirs" that are emptied first as soon as the internal relative humidity decreases. The use of LWA preserves the water in the smaller concrete pores, thus increasing the critical pore radius, r, and decreasing the capillary stress, P_{cap}, in the Laplace equation which effectively reduces the autogenous strain.
- Shrinkage reducing admixtures (SRAs) can be used to reduce autogenous and drying shrinkage. This chemical admixture reduces the surface tension, γ, of the pore solution in the concrete. From the Laplace equation, a lower surface tension will result in a lower capillary tension P_{cap}; therefore, the strain on the paste (ε_p) will also decrease.
- Calcium enrichment can be examined to mitigate the shrinkage in AAS concrete. As explained earlier, the carbonation of AAS materials exacerbates its drying shrinkage strains. AAS is extremely prone to carbonation most likely because of its low C/S ratio

and a lack of CH formation. Introducing a larger concentration of calcium into the material before mixing (by adding $Ca(OH)_2$ powder) may be able to effectively reduce the carbonation rate of these materials.

- The final mitigation strategy involves the reduction of mass transport rate. Drying and carbonation shrinkage are driven by the reaction of concrete with air and the atmosphere. Drying shrinkage occurs when water in the concrete evaporates, and carbonation shrinkage results from the reaction of CO_2 in the atmosphere with the cementitious products. Sealants can be used to impede the transport rate of water and CO_2 to slow down these two types of shrinkage.